UTILIZING HIGH TEMPORAL RESOLUTION STABLE ISOTOPE, SAP-FLUX, AND EDDY COVARIANCE MEASUREMENTS TO PARTITION DAILY EVAPOTRANSPIRATION IN AN OAK WOODLAND

A Thesis

by

CHRISTOPHER ADKISON

Submitted to the Office of Graduate and Professional Studies of
Texas A&M University
in partial fulfillment of the requirements for the degree of

MASTER OF SCIENCE

Chair of Committee,	Georgianne Moore
Co-Chair of Committee,	Caitlyn Cooper
Committee Members,	James Heilman
	Rajit Patankar
Head of Department,	Kirk Winemiller

August 2020

Major Subject: Ecosystem Science and Management

ABSTRACT

The fractional contribution of transpiration (*T*) to total evapotranspiration (*ET*), f_T, is an important indicator of water use efficiency in forests and other ecosystems, and an improved understanding of f_T is necessary for refined water resource management. Recent advancements in cavity ringdown spectrometers have made the collection of high temporal resolution water isotope data possible, yet this technology has not been fully utilized for determining f_T and partitioning *ET*. The primary objective of this study was to effectively partition *ET* in an oak woodland using stable isotopes, sap-flux, and eddy covariance techniques on days where soil and twig sampling provided real values for δ_e and δ_t. We then wanted to model δ_e and δ_t on days when samples were not collected, and to compare the efficacy of using δ^2H versus $\delta^{18}O$ within the stable isotope method. Transpiration was determined by fitting eleven oak (*Quercus stellata* and *Quercus marilandica*) trees with thermal dissipation sap flow sensors and averaging 30-sec measurements over 30-min intervals. Isotope turbulent mixing relationships (Keeling Plots) were used to determine δ_{ET}, while δ_E was calculated using a combination of the Craig-Gordon model and monthly soil and twig samples to verify δ_e and δ_t. It was determined that average daytime vapor pressure deficit (VPD) and soil moisture were the best predictors of δ_e and δ_t, respectively. These models were significant at the 95% confidence level for both stable isotopes for twigs (δ_t), but only $\delta^{18}O$ for soil (δ_e). There was a 41 - 49% overestimation of f_T when utilizing the stable isotope technique compared to T/ET_{EC} or T/ET_0. When normalizing f_T for either $\delta^{18}O$ and δ^2H, the

overestimation was reduced to 4 - 12%, suggesting there may be a systematic bias to the CGM leading to overestimation of f_T in natural systems. When comparing $\delta^{18}O$ and $\delta^{2}H$ within the stable isotope method, there was much agreement between the two, which suggests that higher resolution data can lead to a greater utility of $\delta^{18}O$ in stable isotope studies. However, δ_e models were insignificant during the dormant season, suggesting that the CGM may not perform under these conditions in natural systems.

ACKNOWLEDGEMENTS

I would like to thank my committee chairs, Drs. Georgianne Moore and Caitlyn Cooper, and my committee members, Drs. James Heilman and Rajit Patankar, for their technical, logistical, and practical guidance throughout the course of this research.

I would also like to thank the excellent graduate student community in the department for council, support, and mutual encouragement for excellence and progress. In addition, the department faculty and staff have been nothing short of kind, pleasant, and patient during my tenure at Texas A&M University.

Finally, thanks to my family and friends for the late-night conversations, camping trips, distractions, pep-talks, and all other forms of support that they have provided during this process.

CONTRIBUTORS AND FUNDING SOURCES

Contributors

This work was supervised by a thesis committee consisting of Dr. Georgianne Moore (advisor) of the Department of Ecology and Conservation Biology, Dr. Caitlyn Cooper (co-advisor) of the Department of Rangeland, Fisheries, and Wildlife Management, Professor Dr. James Heilman of the Department of Soil and Crop Science, and Dr. Rajit Patankar of the National Ecological Observatory Network.

The sap flow sensors were built by the student with help from Ashley Cross, Ajinkya Deshpande, Manuel Flores, and Aaron Trimble. The sap flow system was installed by Dr. Caitlyn Cooper, Tian Zhang, Ajinkya Deshpande, and the student.

The eddy covariance and soil moisture data analyzed in Chapter I were collected, cleaned, and made available by the National Ecological Observatory Network. Soil and twig samples discussed in Chapter I were collected with assistance from Ajinkya Deshpande, Aaron Trimble, and Ashley Cross. Samples were extracted and analyzed at the Stable Isotopes for Biosphere Science Laboratory at Texas A&M University by Madison Taylor and Ayumi Hyodo.

Special thanks to Gary Henson and Monika Kelley for maintaining the tower sensors and all other field instrumentation during the tenure of this project. All other work conducted for the thesis was completed by the student independently.

Funding Sources

Graduate study was supported by the Texas A&M University College of Agriculture and Life Sciences Excellence Fellowship, as well as the Department of Ecosystem Science and Management George and Judy Dishman Endowed Graduate Fellowship.

Funding for conferences, travel to field sites, and purchase of research materials were made possible in part by the Office of Graduate and Professional Studies Research and Travel Award, the departmental Graduate Student Travel Grant, and the departmental Graduate Student Research Mini-Grant. The thesis contents are solely the responsibility of the authors and do not necessarily represent the official views of the funding parties.

NOMENCLATURE

CGM	Craig-Gordon Model
CRDS	Cavity Ringdown Spectrometer
DBH	Diameter at Breast Height
E	Evaporation
EC	Eddy Covariance
ET	Evapotranspiration
ET_{EC}	Evapotranspiration from Eddy Covariance Measurements
ET_0	Reference Evapotranspiration from Penman-Monteith
FFP	Flux Footprint
f_T	Fractional Contribution of Transpiration to Total Evapotranspiration
GMWL	Global Meteoric Water Line
IRMS	Isotope Ratio Mass Spectrometer
LBJ	Lyndon B. Johnson National Grassland
NEON	National Ecological Observatory Network
SIBS	Stable Isotopes for Biosphere Science Laboratory
T	Transpiration
TC/EA	Thermo Scientific Temperature Conversion/Elemental Analyzer
USFS	United States Forest Service
VPD	Vapor Pressure Deficit

VWC	Volumetric Water Content
δ_E	Isotopic Composition of Evaporation (‰)
δ_e	Isotopic Composition of Soil Water at the Evaporating Front (‰)
δ_{ET}	Isotopic Composition of Evapotranspiration (‰)
δ_T	Isotopic Composition of Transpiration (‰)
δ_t	Isotopic Composition of Xylem Water Sampled from Twigs (‰)

TABLE OF CONTENTS

Page

ABSTRACT ii

ACKNOWLEDGEMENTS iv

CONTRIBUTORS AND FUNDING SOURCES v

NOMENCLATURE vii

TABLE OF CONTENTS ix

LIST OF FIGURES xi

LIST OF TABLES xiii

CHAPTER I INTRODUCTION 1

- Introduction & Background 1
  - Previous ET Partitioning Work 2
  - Development of Stable Isotopes in ET Partitioning 3
  - Purpose of This Study 5
- Materials and Methods 7
  - National Ecological Observatory Network (NEON) 7
  - Site Description 10
  - Micrometeorology 11
  - Sap Flow Sensors 14
  - Stable Isotopes 23
  - Field Sampling & Sample Analysis 26
  - f_T Analysis for Sampling Days 28
  - Predictive Model Development 29
- Results 30
  - Environmental Data 30
  - Water Fluxes 32
  - Predictive Model 38
  - Entire Growing Season 40
- Discussion 44

CHAPTER II CONCLUSIONS 48

REFERENCES.....49

APPENDIX A INDIVIDUAL VEGETATION PLOT STATISTICS.....61

APPENDIX B SOIL AND TWIG WATER STABLE ISOTOPE COMPOSITION RESULTS.....62

APPENDIX C DESCRIPTIVE STATISTICS FOR LINEAR REGRESSION (KEELING PLOT) ANALYSES FOR EVERY DAY DURING THE GROWING SEASON 64

LIST OF FIGURES

Page

Figure 1. NEON domain and field sites map. LBJ is circled in red. 8

Figure 2. Map of LBJ National Grasslands main section and management units..... 11

Figure 3. FFP Model output for LBJ, May 2019. 13

Figure 4. Map of sap flow trees, eddy covariance tower, and NEON infrastructure. 16

Figure 5. Relationship between sapwood area and basal area for all trees fitted with sap flow sensors. 17

Figure 6. Daily minimum vapor pressure deficit and precipitation with days having a true $\Delta \boldsymbol{Tm}$ marked (A). The raw measured average $\Delta \boldsymbol{Tm}$ and corrected $\Delta \boldsymbol{Tm}$ portraying baseline smoothing (B). 19

Figure 7. Map of the twenty-nine 400-m^2 vegetation plots distributed throughout LBJ. 21

Figure 8. Relationship between tree height and DBH used to gap fill missing DBH data from NEON vegetation surveys for all distributed plots. 22

Figure 9. The total sapwood area per plot for the 29 vegetation plots at LBJ. The black line shows the cutoff point that was used to distinguish between forest and grassland plots. 22

Figure 10. Conceptual diagram for obtaining f_T using the stable isotope method. 24

Figure 11. Thirty-minute average air temperature and wind speed recorded from the EC tower during the study period (A), average daytime (6:00-18:00 h) VPD (B), and soil volumetric water content at 0.16-m depth at soil plot 1 (C). Days where there was an isotope sampling event have been highlighted in yellow 31

Figure 12. Average isotopic composition of water vapor for the study period. The red line indicates DOY 325 when the trees entered dormancy and leaves abscised. 32

Figure 13. Daily transpiration, reference evapotranspiration, actual evapotranspiration, and precipitation for the study period. Days where there was an isotope sampling event have been highlighted in yellow. 33

Figure 14. δ^2H versus $\delta^{18}O$ for soil, precipitation, twig, and atmospheric water samples plotted against the GMWL for the growing season. 34

Figure 15. Inverse water vapor concentration plotted against $\delta^{18}O$ (A) and δ^2H (B) for the 6 sampling events during the growing season. Dashed lines represent linear regressions with *P*-values that were non-significant at α=0.05. 35

Figure 16. The fractional contribution of transpiration to total evapotranspiration on sampling events during the growing season calculated using the stable isotope method for both δ^2H (dark grey bars) and $\delta^{18}O$ (light grey bars), and using the residual of T/ET_0 from scaled sap flow measurements (black bars). 37

Figure 17. Linear regressions of average soil moisture and twig δ^2H (A), average soil moisture and twig $\delta^{18}O$ (B), average daytime VPD and soil $\delta^{18}O$ (C), and average daytime VPD and soil δ^2H (D) for the growing season only. 38

Figure 18. Linear regressions of average soil moisture and twig δ^2H (A), average soil moisture and twig $\delta^{18}O$ (B), average daytime VPD and soil $\delta^{18}O$ (C) and average daytime VPD and soil δ^2H (D) for the growing season data and dormant season data. 39

Figure 19. δ^2H versus $\delta^{18}O$ for soil, precipitation, twig, and atmospheric water samples plotted against the GMWL for the growing season and dormant season data. 40

Figure 20. Fractional transpiration computed using T/ET_{EC} (closed circles), T/ET_0 (open circles) δ^2H (open triangles) and $\delta^{18}O$ (closed triangles)..... 42

Figure 21. Stable isotope f_T normalized to ET_0 (A) and ET_{EC} (B). Data for ET_{EC} before DOY 241 were invalid and excluded from analysis. 43

LIST OF TABLES

Page

Table 1. Summary of data products derived from NEON open-access sources. 9

Table 2. Descriptions of individual trees fitted with sap flow sensors.....18

Table 3. Descriptive statistics for linear regression (Keeling Plot) analyses for sampling events during the growing season. 36

Table 4. Results from *ET* partitioning using the stable isotope approach on sampling days for both $\delta^{2}H$ and $\delta^{18}O$. 36

CHAPTER I

INTRODUCTION

Introduction & Background

Evapotranspiration (*ET*) is an important process in the terrestrial hydrological cycle that accounts for evaporation (*E*) from soil, open water, and canopy-intercepted water and transpired (*T*) water from vegetation. *ET* constitutes a large percentage of the water cycle in most environments, and up to 95% in arid environments (Trenberth et al., 2007; Wilcox et al., 2003). An improved understanding of *ET* dynamics can yield useful information for multiple disciplines, such as hydrology, ecology, meteorology, and biophysics. Furthermore, the terrestrial water cycle, carbon cycle, and energy cycle are all linked via *ET* through various processes such as latent heat fluxes and vegetative primary production (Foley et al., 2003).

An improved understanding of *ET* partitioning and the contribution of *T* to *ET* (f_T) is necessary for refined water resource management and quantification of vegetative responses to climate change and alterations to the carbon cycle. For instance, complex dynamics exist between carbon fluxes and precipitation at multiple scales, and the water-use efficiency of plants varies with ecosystem aridity and vegetation cover (Good et al., 2017).

Partitioning of *ET* is necessary because *T* is seen as a desirable aspect of the water cycle that allows vegetation to grow, while water that is evaporated is generally seen as being “lost” from the system or wasted. Improving scientific understanding of how *ET* is partitioned in different environments and over varying spatial and temporal scales can allow for a more holistic understanding of the climate system as well as vegetative responses to climate change in the future (Helman et al., 2017).

Previous ET Partitioning Work

In a recent review paper, Kool et al. (2014) discussed 52 studies that partitioned *ET* using at least two different techniques. Of these 52 studies, 30 were in field and row crops, 13 were in orchards or vineyards, and only nine studies were in natural vegetated areas such as forests or shrublands. Common methods for computing *ET* at the ecosystem scale include empirical measurements (correlation-based *ET* approach), models (Shuttleworth Wallace, Priestley-Taylor, Penman-Monteith, etc.), and most commonly as the residual of other measurements (water balance approach) with the utilization of stable isotopes rapidly-developing (Ford et al., 2007; Good et al., 2017; Shi et al., 2008; Tie et al., 2018; Williams et al., 2004). Slightly more difficult to execute but still common, methods for actually measuring *ET* at the ecosystem scale include micro-lysimeters, Bowen ratio energy balance, and eddy covariance (EC) techniques (Boast and Robertson, 1982; Bowen 1926; Xiao et al., 2011). Transpiration can be measured at the ecosystem scale by various sap flow measurements such as heat balance (Čermák, Deml, & Penka, 1973; Čermák, Kučera, & Zadezhdina, 2004), heat pulse (Burgess et al., 2001), and heat dissipation methods (Granier 1985, 1987), or by using a biomass-transpiration relationship (Perez-Priego et al., 2010).

Of the studies in natural areas discussed by Kool et al. (2014), six studies used a combination of eddy covariance and sap flow to partition *ET*, and one study used stable isotopes in combination with a model, but no study used the combination of stable isotopes, eddy covariance, and sap flow all together. One study to date has used this particular combination (Williams et al., 2004), but this was in an olive (*Olea europaea*) orchard in Morocco, and not a forest. Aouade et al. (2016) found that stable isotopes seemed to adequately partition *ET* for

winter wheat (*Triticum aestivum*) in Morocco, but the findings were only significant for δ^2H and not for $\delta^{18}O$, the two stable isotopes most commonly measured in ecohydrological research. The reasons for discrepancies between δ^2H and $\delta^{18}O$ were highlighted in Xu et al. (2008) where the stable isotope method was used to partition *ET* in a *Quercus aquifolioides* subalpine shrubland of China. Because the equilibrium enrichment factor (ε_{eq} or ε*) of δ^2H was greater than for $\delta^{18}O$, it made δ^2H more sensitive to evaporative enrichment than $\delta^{18}O$.

Wilson et al. (2001) and Shi et al. (2008) found that EC measurements performed well when compared to traditional methods for measuring *ET*, such as the catchment water balance and the Bowen ratio energy balance, respectively, but Wilson et al. (2001) reported *T* being underestimated by sap flow, likely due to issues with scaling up *T* from ring-porous tree species (*Quercus* and *Acer*) and capturing the EC tower footprint. Others such as Moore, Cleverly, & Owens (2008) have noted that nighttime transpiration can be an important factor in *ET* studies, and the traditional heat dissipation equation assumes that flows reach zero every night (Granier 1985, 1987). In systems where vapor pressure deficit (VPD) remains high throughout the night and adequate soil moisture is present, nighttime flows can introduce a significant amount of error in *T* estimation. Furthermore, some studies have reported diurnal and seasonal differences between EC measurements and other techniques such as stable isotopes (Williams et al., 2004) while others have found the estimates to be similar (Shi et al., 2008).

Development of Stable Isotopes in ET Partitioning

The use of stable isotopes in ecohydrology research has made significant progress since the inception of mass spectrometry in the 1960's and 1970's (Nier, 1991). Initial experiments in *ET* partitioning-related research specifically date back to the 1990's with Jean-Pierre Brunel

being among the first to fully utilize the technique (Brunel et al., 1991, 1995, 1997; Walker & Brunel, 1990). These experiments were conducted in semi-arid environments of south-eastern Australia and the Sahel region of Africa with the isotopic composition of atmospheric water vapor being sampled using refrigerated traps manually deployed for 2 - 4 hours at a time before transferring the water to glass vials for lab analysis. This same method is still used for collecting water vapor in more recent studies as well (Aouade et al., 2016; Williams et al., 2004).

Early work from Brunel et al. (1995) that has been expanded upon adequately captures isotopic composition at short temporal scales, but the need for higher resolution, more convenient approaches for sampling water vapor isotopes is apparent for studies lasting longer than just a few days, or when many measurements are needed continuously throughout a single day. These challenges brought about the use of cavity ringdown spectrometers (CRDS) in the field, which are now the preferred method due to their simplicity, ease of use, and high temporal resolution capabilities. Picarro™ and Los Gatos Research sell field deployable units commercially, and these are the most widely used. Their use has started to increase in the last decade in a variety of ecosystem types, though their relatively high price and need for infrastructure and constant calibrations can pose logistical and economic constraints to their utility (He et al., 2018; Pierchala et al., 2019; Wang et al., 2010). They operate by using a semiconductor diode laser directed into a 35 cc cavity, which then circulates ~100,000 times between three mirrors (equivalent of up to 20 km) and the decay of energy is measured, and is directly proportional to the concentration of gas in the sample injection.

There is good agreement between results from CRDS and Isotope Ratio Mass Spectrometry (IRMS) studies, indicating that the dual use of both methods in a single study will not compromise the interpretability of the results (Munksgaard et al., 2011). Liquid water from

soil and twig samples used as other end members in isotopic studies are generally analyzed using IRMS (Williams et al., 2004; Xiao et al., 2018; Zhang et al., 2010).

Purpose of This Study

Evapotranspiration was measured and partitioned in an oak woodland located in the Lyndon B. Johnson (LBJ) National Grassland in Decatur, TX, using stable isotope, sap-flux, and eddy covariance techniques. Working in this region is significant due to the Cross Timbers being a transition zone between the humid mixed deciduous/pine forests to the east, and semi-arid prairies and shrublands to the west (Hoff et al., 2018). There has been interest in documenting the changing forest structure of the Cross Timbers, namely woody encroachment by eastern red cedar (*Juniperus virginiana* L.), and a better understanding of *ET* dynamics in these systems is warranted. Transpiration in oaks from other parts of the world have been studied (Cooper et al. 2019; Poyatos et al., 2005; Poyatos et al., 2007; Yan et al., 2016), but the sap-flux responses of the oaks in LBJ are uncertain. These oaks are an ideal system to partition because in addition to occurring in the dry western extent of eastern deciduous forests, they have a relatively open canopy similar to that of a savanna. Water limitation on *T* is a critical factor influencing the stand structure and function in this system.

The National Ecological Observatory Network (NEON) maintains a research site at LBJ where they have deployed a large variety of scientific instrumentation and data collection infrastructure to capture continuous carbon and water fluxes for the next 30 years (National Ecological Observatory Network, 2020). Of the instruments currently in operation, they have an EC tower which collects high-resolution micrometeorological information at five different heights in the forest canopy, as well as a cavity ringdown spectrometer that analyzes isotopic

composition of water vapor at each of the five heights in real time. In addition to the NEON instrumentation, I installed a sap flow system in May of 2019 to collect transpiration data on blackjack oak (*Quercus marilandica* Muenchh) and post oak (*Quercus stellata* Wangenh) to compare with the stable isotope and EC data. Additionally, monthly twig and soil samples were collected to characterize the isotopic composition of transpired and evaporated water, respectively, information necessary to partition *ET* using the stable isotope method.

Objectives

The primary objective of this study is to effectively partition *ET* in an oak woodland using stable isotopes, sap-flux, and eddy covariance techniques on days where soil and twig sampling provide real values for δ_e and δ_t. This particular combination of techniques has not been utilized in an oak woodland, and having a system that collects data for multiple months will provide insight into how f_T changes over the seasons. Only two studies using the isotopic method have been over an entire growing season or longer, and these were in croplands not forest (Sun et al., 2019).

In order to advance the stable isotope method for ET partitioning, the next objective is to create δ_e and δ_t predictive models for partitioning daily *ET* on non-sampling days using a combination of monthly field samples, 30-min transpiration, soil moisture, precipitation, vapor pressure deficit (VPD), and water vapor isotopes, along with total daily *ET*. This type of model has not yet been developed for the stable isotope *ET* partitioning method and could prove extremely useful for future studies where sampling soil and twigs at the daily scale is not feasible. This type of model could be used at other forested sites, and particularly at all NEON terrestrial sites.

Using the two stable isotopes of water, I will compare the efficacy of δ^2H and $\delta^{18}O$ in partitioning *ET* using the stable isotope method. Most studies have indicated that δ^2H is better for *ET* partitioning due to its sensitivity to evaporative enrichment compared to $\delta^{18}O$. The CRDS collects continuous data for both isotopes, but many isotope studies have not had that ability to compare the two (Sun et al., 2019). Lastly, I will compare *T* estimated from scaled sap flow measurements to *T* from isotope partitioned *ET*. There is a fair amount of disagreement between scaled sap flow *T* and other estimates of *T* (Williams et al., 2004; Wilson et al., 2001), however, a higher data resolution at LBJ may provide a novel degree of agreement.

Materials and Methods

National Ecological Observatory Network (NEON)

This research was conducted in partnership with the National Ecological Observatory Network (funded by the National Science Foundation and operated by Battelle) who allowed our team access to the research site and provided support services for this work. NEON operates a total of 81 aquatic and terrestrial sites located in 20 different ecoregions of the United States (Figure 1) and collects standardized data at uniform timescales using consistent methods with the goal of providing insight into ecosystem processes, structure, and function (National Ecological Observatory Network, 2020). Data is collected through automated in-situ instruments, periodic observational sampling, and with airborne remote sensing. All data is then checked for quality assurance by NEON staff and provided to the public for free on their website. A summary of NEON data products used in this study can be found in Table 1.

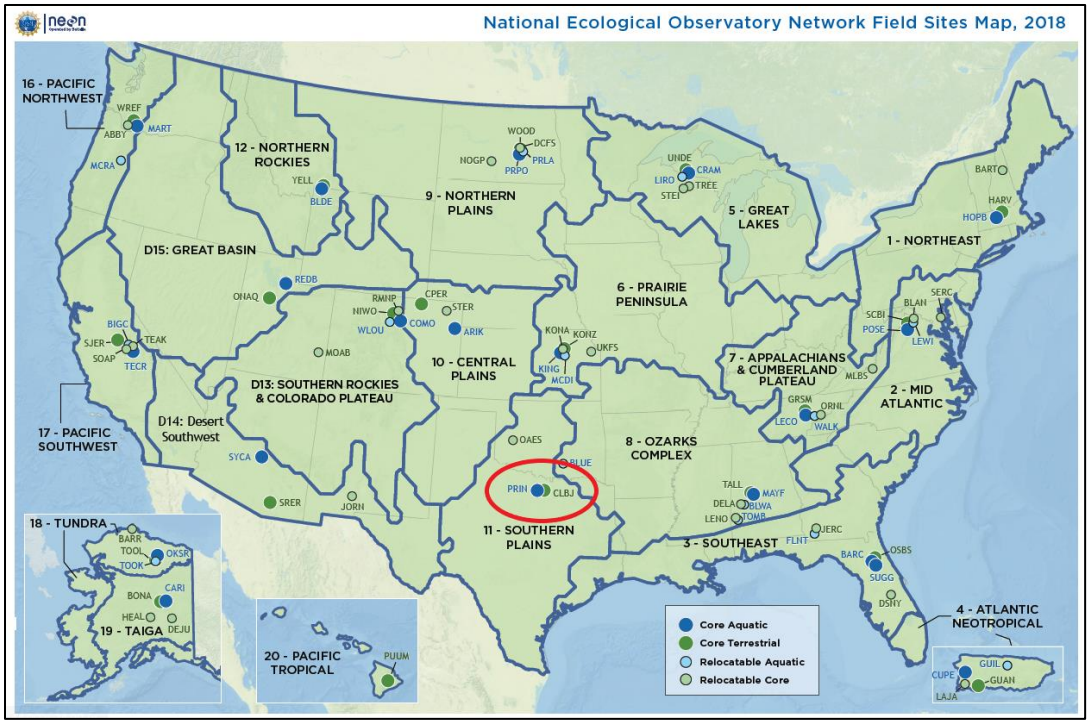

Figure 1. NEON domain and field sites map. LBJ is circled in red.

Table 1. Summary of data products derived from NEON open-access sources.

Data Product	Used In	Instrument	NEON Product Code
Isotopic composition of ecosystem boundary layer (TL 1-4)	Keeling Plot & GMWL	PICARRO L2130-i	DP1.00037.001
Water vapor concentration of ecosystem boundary layer (TL 1-4)	Keeling Plot	LI-840A	DP1.00100.001
Isotopic composition of planetary boundary layer (Tower Top)	Keeling Plot, GMWL, & CGM	PICARRO L2130-i	DP1.00037.001
Water vapor concentration of planetary boundary layer (Tower Top)	Keeling Plot	LI-840A	DP1.00100.001
Relative humidity	CGM & VPD	HMP155A (Tower Top)	DP1.00098.001
Soil moisture	Predictive Model	Sentek - EnviroSCAN TriSCAN	DP1.00094.001
Air temperature	VPD	Thermometrics Climate RTD 100 Ω Probe	DP1.00002.001
Latent heat flux	Total Evapotranspiration	LI-7200/LI-840A/CSAT-3 3D Sonic Anemometer	DP4.00137.001
Shortwave and longwave radiation (Net radiometer)	Penman-Monteith Model	Hukseflux NR01 Net Radiometer	DP1.00023.001
Soil heat flux	Penman-Monteith Model	Hukseflux HFP01SC: Self-Calibrating Heat Flux Sensor	DP1.00040.001
2D Wind speed and direction	Penman-Monteith & FFP	Gill - Wind Observer II; Extreme Weather Wind Observer	DP1.00001.001
Precipitation	Sap Flow Analysis	Belfort AEPG II 600M Weighing gauge (DFIR)	DP1.00006.001
Stable isotope concentrations in precipitation	GMWL	N-Con Systems Company Wet Deposition Collector	DP1.00038.001
Woody plant vegetation structure (DBH & Species)	Sap Flow Analysis	Field Crew	DP1.10098.001

Site Description

The study site is located within management unit 75 of LBJ National Grasslands in Wise County, TX located just north of the city of Decatur, TX (Figure 2). It is a core terrestrial site in NEON's Southern Plains domain (D11) (Figure 1). LBJ is considered part of the Cross Timbers ecoregion of Texas, and forested areas within the park consist mostly of mixed oaks (*Quercus* spp.), elms (*Ulmus crassifolia* and *Ulmus alata*), eastern red cedar, and sugarberry (*Celtis laevigata*) with a mean canopy height of 3.96 m. Dominant forest species in the immediate vicinity of the eddy covariance tower are blackjack oak and post oak. LBJ is located within the Trinity River Basin, and the study site is situated near two smaller tributaries (Denton Creek and Cottonwood Creek) that flow just outside the perimeter of management unit 75. Elevation of the area is 259 m above sea level, and the EC tower is located precisely at 33.40123°N, -97.57°W (Figure 3).

Soils consist of Keeter very fine sandy loams (1 - 6 percent slopes) and Duffau-Weatherford Complex (3 - 8 percent slopes) (Soil Survey Staff, 2019). Mean annual temperature is 18°C and peak temperatures usually occur in August, while mean annual precipitation (MAP) is 840 mm $year^{-1}$ with a bimodal distribution (rainy seasons in late spring and fall) (National Ecological Observatory Network, 2020). Mean annual potential evapotranspiration (PET) and runoff are 1,785 mm $year^{-1}$ and 8 mm $year^{-1}$ respectively (Wine & Hendrickx, 2013)The site has undergone prescribed burning for two consecutive years (2017 & 2018) during spring as a strategy to control the thick understory of greenbrier (*Smilax rotundifolia*).

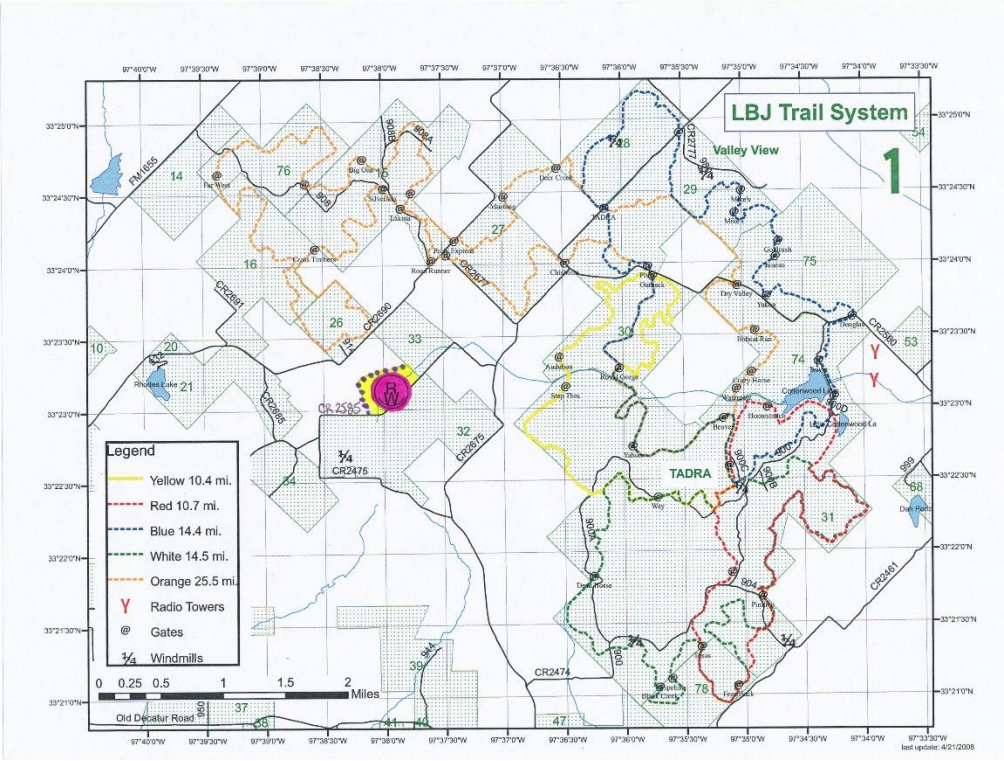

Figure 2. Map of LBJ National Grasslands main section and management units.

Micrometeorology

The EC method is increasingly used in studies of micrometeorology and biophysics as a method for measuring high-frequency gas fluxes and latent heat (Perez-Priego et al., 2017; Shi et al., 2008; Zitouna-Chebbi et al., 2018). While it was originally developed over 30 years ago, changes in methodology and improvements in instrumentation have made it a highly defensible and accurate method that is preferred in most micrometeorological studies (Burba, 2013). At LBJ, NEON operates an EC tower that is fitted with instruments at four different heights in the forest canopy, with one set of sensors extending above the canopy as well. These instruments include a sonic

anemometer, net radiometer, open-path CO_2/H_2O analyzer, as well as tubing that collects vapor at each level and directs it inside the instrument hut for isotopic analysis on the Picarro™ CRDS.

All data products and associated metadata produced from the EC tower were delivered in an HDF5 file format. Downloading and analyzing this data requires a free proprietary software published by the HDF Group (found at https://www.hdfgroup.org/). After being extracted from HDF5 file format, data were then analyzed and managed using Microsoft Excel and RStudio (R Core Team, Vienna, Austria).

Latent Heat Flux

Actual evapotranspiration (ET_{EC}) values were converted from the given latent heat flux (λE, $W \cdot m^{-2}$) values to mass units ($mm \cdot day^{-1}$) using the latent heat of vaporization of water and Equation 1 for every 30 minutes and then summed over the course of 24 hours. Days where there were not at least 40/48 data points available were excluded from analysis.

$$\frac{W}{m^2} = \frac{J}{m^2 \cdot s} \times \frac{1\ kg}{2454000\ J} \times \frac{60\ sec}{1\ min} \times \frac{60\ min}{1\ hour} \times \frac{24\ hours}{1\ day} = \frac{kg}{m^2 \cdot day} \times \frac{1\ liter}{1\ kg} \times \frac{0.001\ m^3}{1\ liter} \times \frac{1000\ mm}{1\ m} = \frac{mm}{day} \quad (1)$$

Flux Footprint Modeling (FFP)

To accurately scale up *T* to the area of the EC tower, the flux footprint area must be known. This was modeled using the Kljun et al. (2015) FFP Model (found at https://geography.swansea.ac.uk/nkljun/ffp/www/). Input data for the model include wind speed, wind direction, friction velocity, Obukhov length, displacement height, measurement height, and standard deviation of lateral velocity fluctuations after rotation. These parameters were all included in the NEON Eddy Covariance Data Bundle,

excluding the Obukhov length. However, this was estimated using the friction velocity and the equation

$$L = A \times u^{*2} \quad (2)$$

where L is Obukhov length, A is 1,100 s^2 m^{-1}, and u^* is friction velocity (Venkatram, 1980). The results of the FFP model from May 2019 can be seen in Figure 3, with red contour lines representing the confidence of the flux footprint falling within that area. The 70% confidence line was utilized for scaling up *T* estimates from tree to ecosystem level due to there being complete forest cover within this boundary.

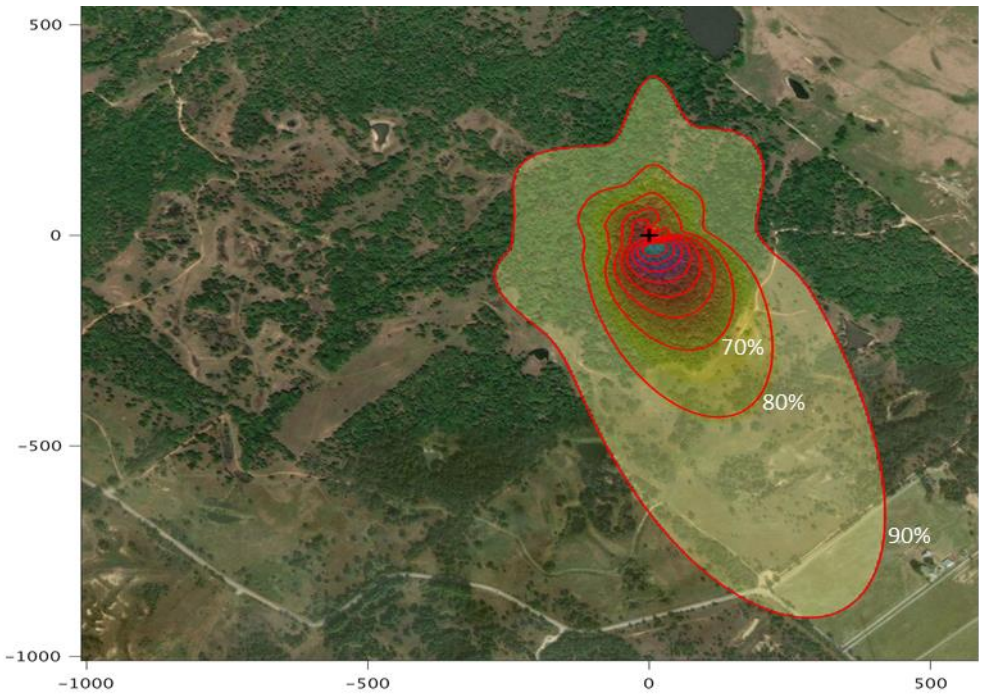

Figure 3. FFP Model output for LBJ, May 2019.

Penman-Monteith

Due to EC sensor issues in the beginning of the study, the Penman-Monteith reference evapotranspiration (ET_0; mm·day^{-1}) was calculated to provide *ET* estimates. The FAO-56 method (Zotarelli et al., 2018) was utilized at the daily scale using the equation

$$ET_0 = \frac{0.408\Delta\,(R_n - G) + \gamma \frac{900}{T+273} u_2 (e_s - e_a)}{\Delta + \gamma(1 + 0.34u_2)} \quad (3)$$

where Δ is the slope of vapor pressure curve (kPa·°C^{-1}), R_n is net radiation (MJ·m^{-2}·day^{-1}), G is soil heat flux (MJ·m^{-2}·day^{-1}), γ is the psychometric constant (kPa·°C^{-1}), T is air temperature at a height of 2-m (°C), u_2 is wind speed at a height of 2-m (m·s^{-1}), and e_s-e_a is the vapor pressure deficit (kPa). If there were incomplete data (<40 data points) for any of the input parameters then that day was excluded from analysis. Air temperature and wind speed was averaged from measurements of the five different heights on the EC tower at 30-min intervals.

Sap Flow Sensors

To directly measure transpiration in the EC tower footprint, eleven oak trees were fitted with thermal dissipation sap flow sensors (Granier, 1985, 1987) in May 2019 and have been running continually since then. The location of trees for use in sap flow measurements can be seen in Figure 4 along with the EC tower, soil arrays, and the instrument hut. All instrumented trees were either *Quercus marilandica* or *Quercus stellata* with a minimum, maximum, and average diameter at breast height (DBH) of 21.5, 54.5, and 32.6 cm respectively (Table 2). All trees selected for instrumentation

were within the specified buffer delineated by the NEON permit at LBJ to negate the need for additional research permits through the USFS. All trees had branches above sensor installation height (~ 1.3 m) and were not shaded by any nearby tree.

Sap flow sensors were custom made in the Moore Ecohydrology Lab at Texas A&M University by cutting a stainless-steel needle to 2-cm in length and inserting a copper-constantan thermocouple into the needle. A window was created at 1 cm using a Dremel tool and the soldered end of the thermocouple was fastened into place using super glue in the window. For the heaters, an additional constantan wire was wrapped around the needle approximately 40 times to create a coil. Each tree contained two sensors (or four probes) with one placed on the east side of the tree and one on the west side. Sensors were inserted into the sapwood of the tree to 2-cm depth and connected together in opposition. Sensor heating was controlled by an AVRD voltage regulator (Dynamax Inc., Houston, TX). Data was collected every 30 seconds and later averaged over 30-minute intervals before being stored in *.dat format on a CR1000 datalogger (CR1000, Campbell Scientific Inc., Logan, Utah) before being transmitted to a desktop in College Station, TX for remote access and data screening.

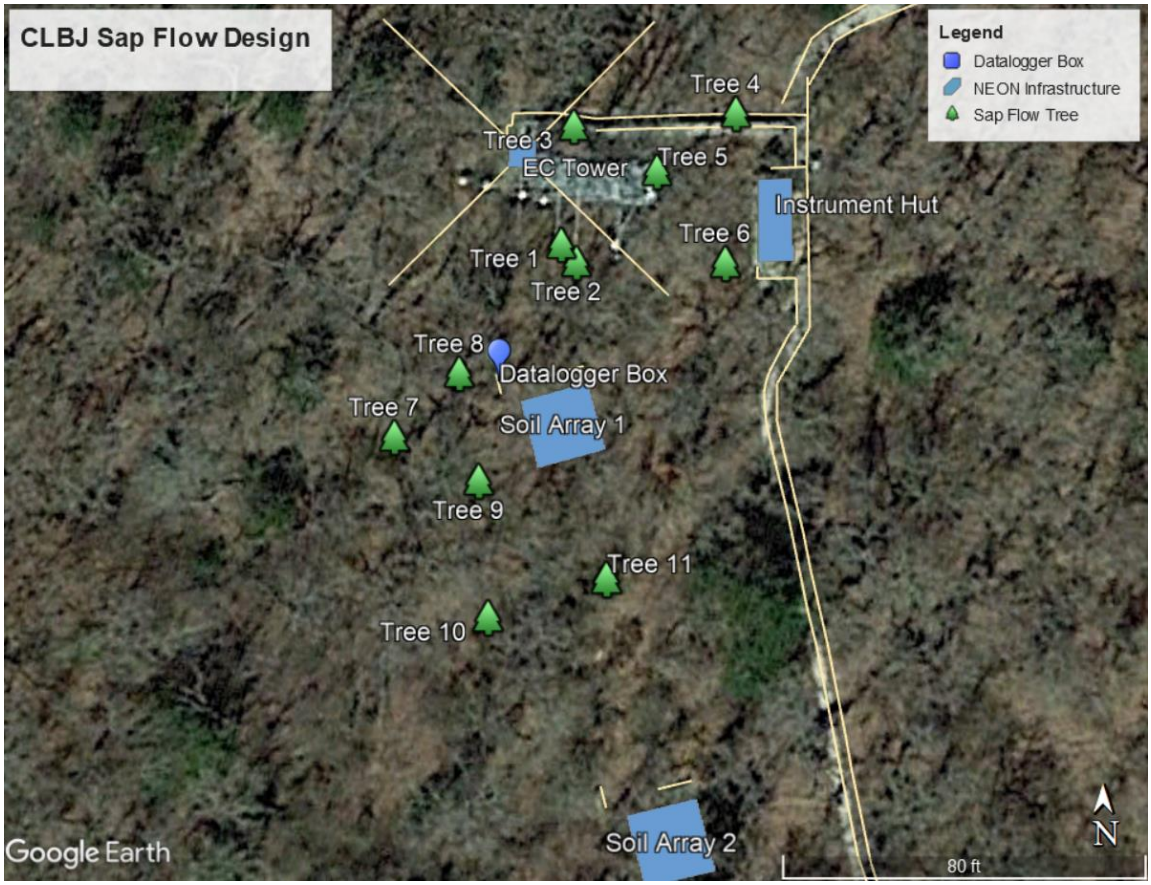

Figure 4. Map of sap flow trees, eddy covariance tower, and NEON infrastructure.

The Granier-style probes used in the study were based off of the thermal dissipation method where two probes are inserted radially into the outer sapwood of a tree to a depth of 2 cm. The top probe (heater) is constantly heated and the bottom probe (reference) is not. The difference in temperature between the heater and reference probes (ΔT) is related to sap flow velocity by the equation

$$J_s = 0.119 \left(\frac{\Delta T_m - \Delta T}{\Delta T}\right)^{1.231} = 0.119K^{1.231} \quad (4)$$

where J_s is the sap-flux density ($kg \cdot m^{-2} \cdot day^{-1}$), ΔT_m is the temperature difference between heater and reference probe at zero flow ($J_s = 0$), and ΔT is the temperature difference between the heater and reference at positive flow ($J_s > 0$) (Granier, 1985, 1987).

The total sap flow of the tree (F) was calculated using the equation

$$F = J_s S_A \quad (5)$$

using sap-flux density (J_s) and the cross-sectional area of the sapwood (S_A) where the heater was inserted . The sapwood depth was determined by taking tree cores using an increment borer and partially immersing the fresh cores in a safranin-fucsin dye (Vertessy et al., 1995; McDowell et al., 2002; Gebauer et al., 2008). Where the dye clearly moved from the bottom to the top of the core was considered to be actively conducting sapwood. All trees with sensors had a sapwood radius greater than the sensor depth of 20 mm (Table 2) (Clearwater et al., 1999). Sapwood area ranged from 0.022 to 0.149 m^2 with an average of 0.056 m^2.

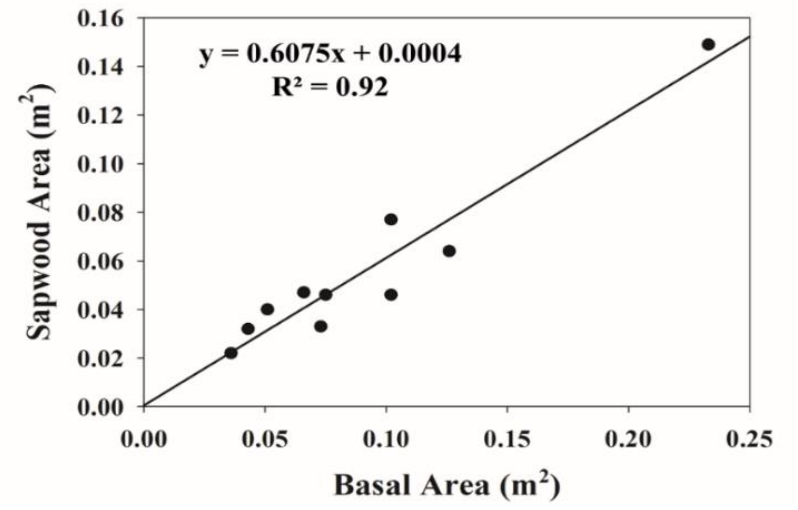

Figure 5. Relationship between sapwood area and basal area for all trees fitted with sap flow sensors.

Table 2. Descriptions of individual trees fitted with sap flow sensors.

Tree #	DBH (cm)	Basal Area (cm^2)	Sapwood Area (cm^2)
1	23.5	434	320
2	25.5	511	399
3	30.5	731	326
4	36.0	1018	773
5	40.0	1257	639
6	54.5	2333	1490
7	36.0	1018	457
8	29.0	661	474
9*	31.0	755	--
10	31.0	755	459
11	21.5	363	222

* Tree 9 was rotten and not cored on this date

Baseline Corrections

It was determined after initial calculations of vapor pressure deficit (VPD) and sap flow processing that nighttime flows were occurring at the site. VPD did not reach zero on a nightly basis and there was not a consistent baseline for ΔT_mwhich introduces error into the original thermal dissipation equation (Equation 4). To account for this error and adjust ΔT_m for nighttime flows, a "baseline smoothing" process was utilized where daily minimum VPD was plotted with daily precipitation (Figure 6A) and days that had <0.1 kPa VPD and zero precipitation were considered days where calculated $\Delta T_m$was accurate. These were used as "anchor points" and the ΔT_m for days in-between were linearly gap-filled to create a smooth baseline. The original ΔT_m was then subtracted from the adjusted $\Delta T_m$to ensure there were no negative values, and if there were the original ΔT_mwere used (Figure 6B). These new ΔT_mwere then used to re-process the sap flow data with Equation 4.

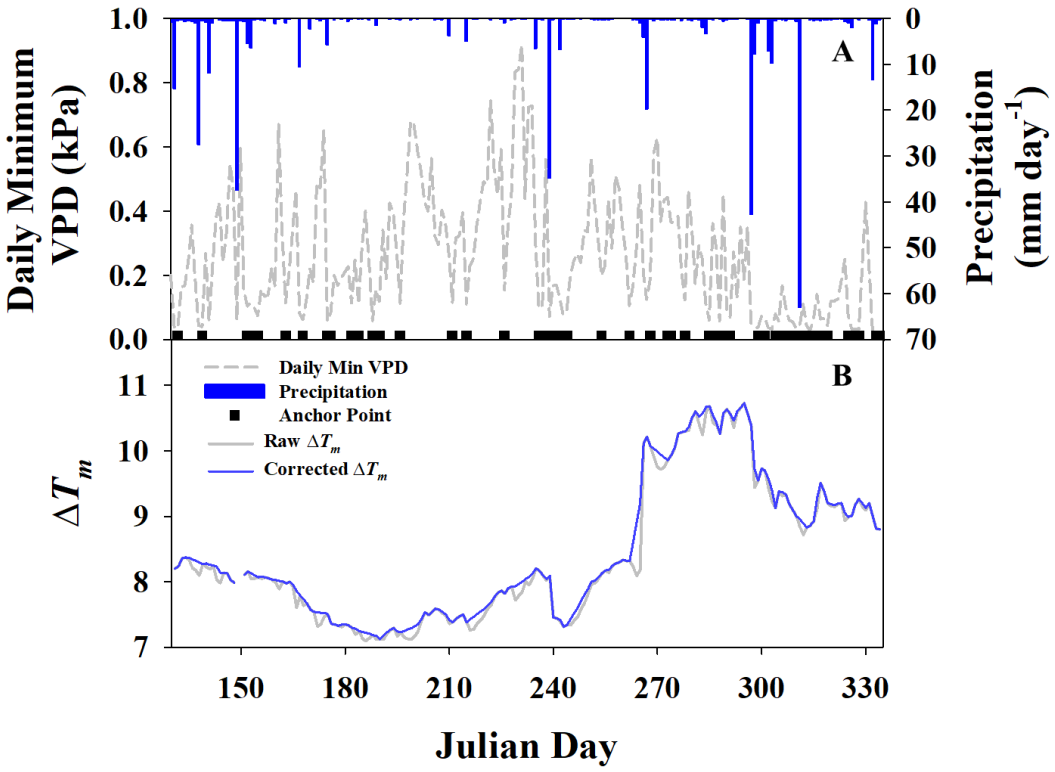

Figure 6. Daily minimum vapor pressure deficit and precipitation with days having a true ΔT_m marked (A). The raw measured average ΔT_m and corrected ΔT_m portraying baseline smoothing (B).

Transpiration Scaling

Scaling up sap flow measurements to the footprint of the EC tower was done using detailed survey information from trees in 29 individual 400-m^2 vegetation plots collected by NEON staff (Figure 7). Within the 29 plots, there were 915 live individuals total for which the stem diameter and tree height were recorded. A power law was used to predict the DBH based on tree height to gap fill missing data (Figure 8). Using DBH, the basal area was then calculated for each individual tree and the allometric equation from Figure 5 was applied to calculate the sapwood area for each individual. The total

sapwood area per plot was divided by the total plot area to get sapwood area per unit ground area ($m^2\ m^{-2}$) for each plot, and a threshold value of 0.2 m^2 of sapwood area was used to differentiate between forest and grassland plots (Figure 9, Appendix A). The average sapwood area per unit ground area for all of the forest plots ($\bar{x}$ = 0.0012 $m^2\ m^{-2}$ ± 0.0006, n = 19) was used to calculate the total sapwood area in the EC tower airshed. Transpiration (mm day^{-1}) was then calculated by multiplying the average sap-flux density of all sap flow trees (kg $m^{-2}\ day^{-1}$) by the average sapwood area per unit ground area. This bottom-up approach has been utilized in other studies (Ford et al., 2007; Williams et al., 2004) and validated by a review on methods for scaling up *T* measurements from tree to stand level (Mackay et al., 2010). It should be noted that this *T* estimate was based on oak allometry and sap-flux of oaks, and there were other species present in the plots as well that may have a different proportion of sapwood area to basal area and sap-flux rates that were being treated like they were oaks. However, no understory species were included in this *T* estimate and any woody vegetation with a DBH smaller than 0.5 cm were not included.

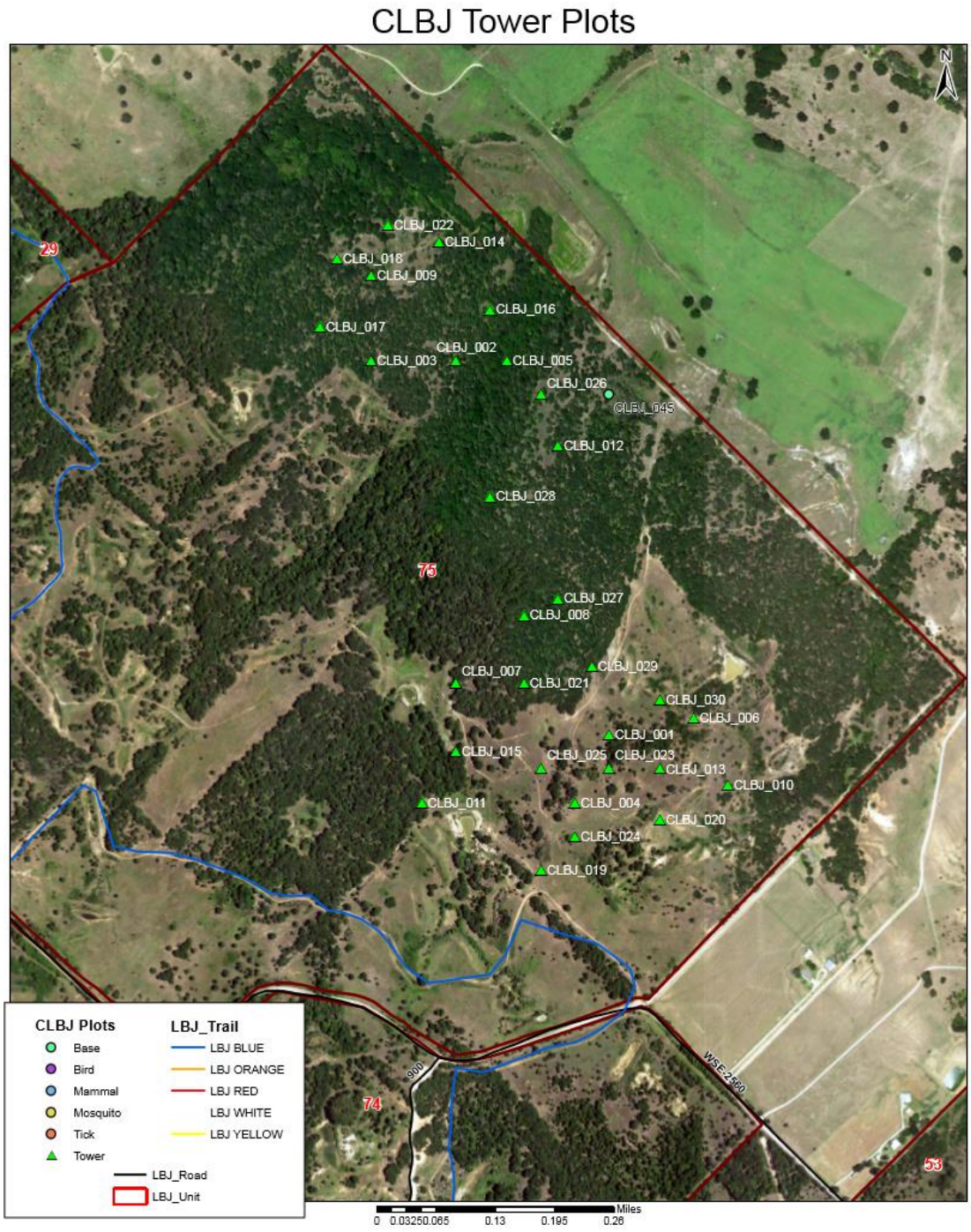

Figure 7. Map of the twenty-nine 400-m^2 vegetation plots distributed throughout LBJ.

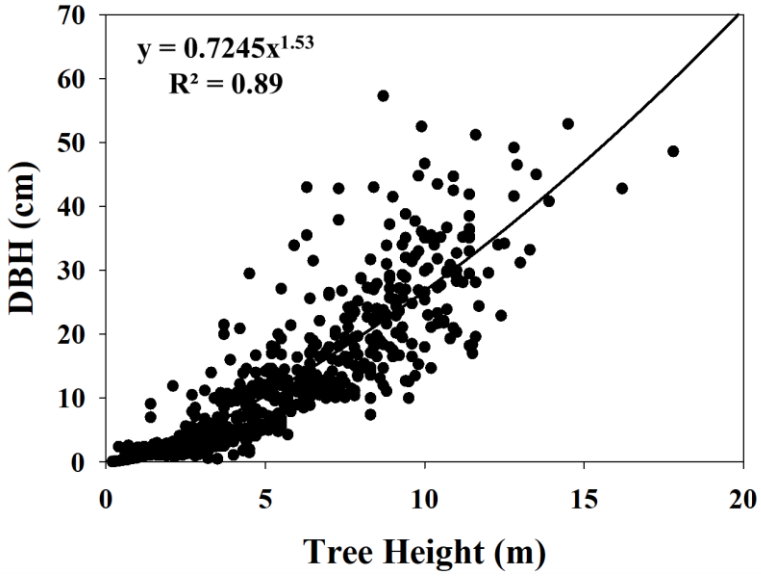

Figure 8. Relationship between tree height and DBH used to gap fill missing DBH data from NEON vegetation surveys for all distributed plots.

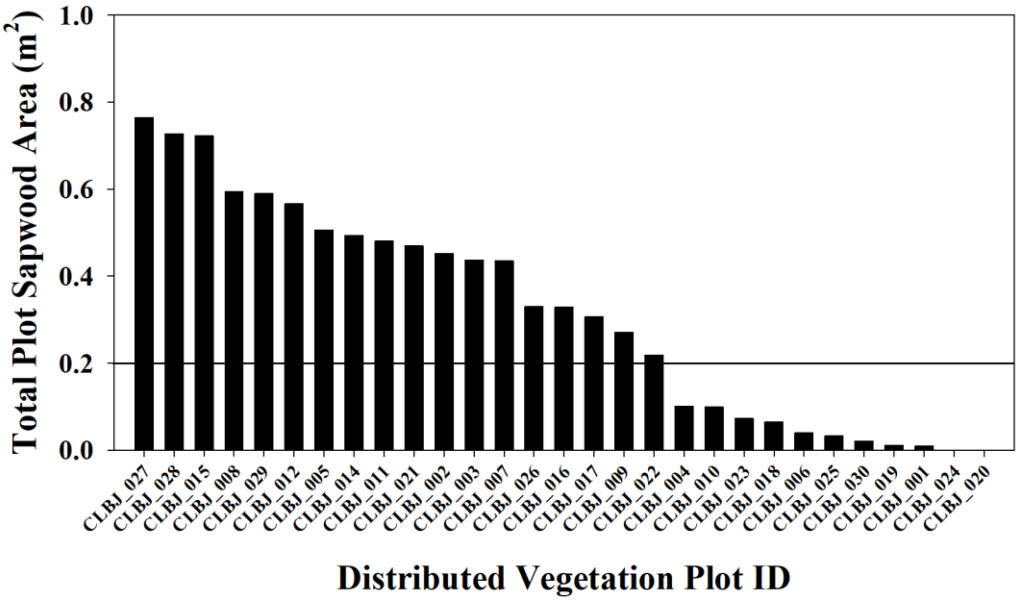

Figure 9. The total sapwood area per plot for the 29 vegetation plots at LBJ. The black line shows the cutoff point that was used to distinguish between forest and grassland plots.

Stable Isotopes

Method Framework

The use of water stable isotopes for partitioning of *ET* has been used widely in the past and is a powerful tool that can be utilized at various scales. Combined with traditional methods for measuring total ecosystem *ET*, the respective contributions of *T* and *E* to *ET* can be calculated using the isotopic mass balance approach, assuming a two-source model

$$\delta_{ET} ET = \delta_E E + \delta_T T \quad (6)$$

where δ_{ET}, δ_E, and δ_T are equal to the isotopic composition of evapotranspiration, soil evaporation, and plant transpiration, respectively. The ratio of *T* to *ET* can then be calculated as

$$f_T = \frac{T}{ET} = \frac{\delta_{ET} - \delta_E}{\delta_T - \delta_E} \quad (7)$$

To use this method, the isotopic composition of water in three "end members" (i.e. soil, vegetation, and atmosphere) are needed, and the resulting ratios of each can be applied to total *ET* to get values of the individual components (Xiao et al., 2018; Zhang et al., 2010). Differences in the isotopic composition of water in vegetation and in soil occur from fractionation during the evaporation process, where the lighter isotopologues of water ($^1H_2{}^{16}O$) leave the evaporation front and the heavier isotopologues ($^1H_2{}^{18}O$ and $^1H^2H^{16}O$) accumulate, leaving the soil water "enriched". The soil evaporating front changes with soil texture, soil moisture, and other environmental conditions, but is generally at the surface when soil is saturated, and between 0.2 - 0.3 m in depth when the soil is not saturated (Barnes and Allison, 1988; Sprenger et al., 2016; Zimmerman et

al., 1967). Water is not fractionated during the transpiration process under steady state conditions, so the isotopic composition of transpired water can be assumed equal to that of the xylem water (Brunel et al., 1995; Ehleringer and Dawson, 1992; Yepez et al., 2003). Steady state conditions are usually met around midday in field conditions (Flanagan et al., 1991). Figure 10 shows the stepwise process for partitioning *ET* using the stable isotope method.

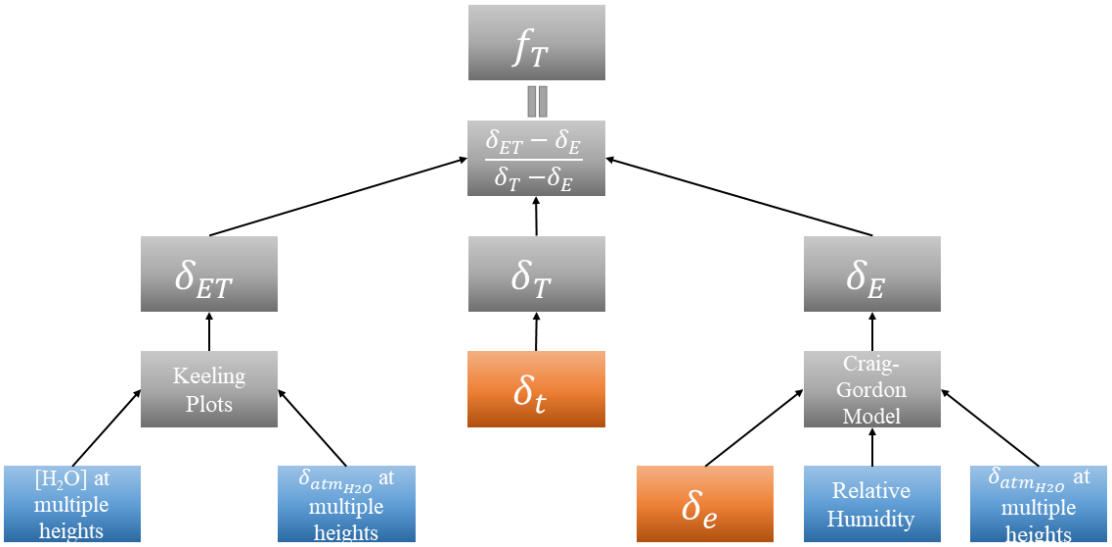

*All δ values can be either δ^2H or $\delta^{18}O$.
** Blue boxes are 30-min NEON data, red boxes are monthly samples.
δ_e= isotopic composition of soil water at evaporating front, obtained from soil samples.
δ_t= isotopic composition of xylem water, obtained from twig samples collected under steady-state conditions.

Figure 10. Conceptual diagram for obtaining f_T using the stable isotope method.

δ_{ET}

The Keeling plot approach is the most commonly used method for obtaining δ_{ET} (Xiao et al., 2018). Measurements of the concentration and isotopic composition of water vapor at varying heights in the forest canopy are sufficient to fit the linear model

used in the Keeling plot approach (Keeling, 1958, 1961; Yakir and Sternberg, 2000). Using linear regression, if δ_{ebl}, C_{pbl}, and δ_{pbl} are measured, then the y-intercept (δ_{ET}) can be solved for using the equation

$$\delta_{ebl} = C_{pbl}(\delta_{pbl} - \delta_{ET})(\frac{1}{C_{ebl}}) + \delta_{ET} \quad (8)$$

where δ_{ebl} is the isotopic composition of the ecosystem boundary layer, C_{pbl} is the water vapor concentration in the planetary boundary layer, δ_{pbl} is the isotopic composition of the planetary boundary layer, δ_{ET} is the isotopic composition of evapotranspiration, and C_{ebl} is the water vapor concentration in the ecosystem boundary layer.

The information needed for this approach were collected by NEON and given on their website (National Ecological Observatory Network, 2020). Water vapor was collected by tubing at five different heights on a 30-minute timestep in the forest canopy and circulated into the instrument hut where it was then analyzed for $\delta^{18}O$ and $\delta^{2}H$ via cavity ring-down spectroscopy (Picarro L2130-i, Picarro Inc., Santa Clara, CA) in near-real time. Water vapor concentrations at the same heights were included in the bundled EC data products published by NEON. Only values from 10:30-14:00 h were used in the analysis.

δ_E

Values of δ_E were attained from a combination of field samples and the Craig-Gordon Model shown below (Craig and Gordon, 1965).

$$\delta_E = \frac{\delta_e/\alpha^* - h\delta_v - \varepsilon_{eq} - (1-h)\varepsilon_k}{(1-h) + (1-h)\varepsilon_k/1000} \quad (9)$$

where δ_e is the isotopic composition of liquid water at the soil evaporating front, α^* is the equilibrium fraction factor (1.0098 and 1.084 at 20ºC for ^{18}O and ^{2}H, respectively (Majoube, 1971)), h is relative humidity, δ_v is the isotopic composition of the background atmospheric water vapor, α_k is the isotopic fractionation factor (0.9755 and 0.9723 for ^{2}H and ^{18}O, respectively (Cappa et al., 2003; Merlivat, 1978)), ε_{eq} is equal to $1000(1-1/\alpha^*)$, and ε_k is equal to $1000(\alpha_k-1)$.

δ_T

Values for δ_T were attained directly through sampling of twig water under steady state assumptions, and many studies have estimated δ_T in this way (Xiao et al., 2018). Under this scenario, it is assumed that the isotopic composition of the source water and transpired water are the same ($\delta_X = \delta_T$).

Field Sampling & Sample Analysis

Soil & Twig Sampling

To obtain isotopic values for soil water at the evaporating front (δ_e) and xylem water (δ_t), monthly soil and twig samples were taken. There was a total of nine sampling events during the study period that were carried out approximately every four weeks (DOY 143, 170, 204, 234, 266, 294, 329, 351, 24). Soil samples (n = 4 per sampling day) were collected at midday (between 10:30 - 14:00 h) every month during the period of the study (May 2019 – January 2020) to capture seasonal variability in δ_E. Samples were collected at 0.2 to 0.3-m depth within the 0.5-m buffer around NEON soil arrays 1 & 2 (Figure 4) when soil was unsaturated, and taken from the surface when soil was

saturated. Soil saturation was determined at the site on sampling days before cores were taken. Samples were taken using a hand auger and immediately transferred into 12-mL glass vials and sealed with a cap and parafilm. To prevent evaporation, vials were stored upside down and placed in a cooler with ice packs (~34 °C) before being transported back to Texas A&M University for storage in a freezer. The time from sampling to storage did not exceed 8 hours at any time. Samples were kept in the freezer until all samples for the season were taken, and then they were transported to the Stable Isotopes for Biosphere Science (SIBS) Laboratory at Texas A&M University.

Twig samples (n = 4 per sampling day) were collected on the same days as soil samples in the same time window to satisfy steady-state conditions for xylem water sampling and to capture seasonal variability in δ_T. Samples were taken using a pole pruner from mature branches on trees containing sap flow sensors and were approximately three to five centimeters in length and a few centimeters in diameter. The bark was then stripped from the twigs, and the twigs were immediately transferred into 12-mL glass vials and stored in the same manner as the soil samples.

Cryogenic Water Extractions & Analysis

All samples underwent water extractions using a cryogenic (liquid nitrogen) vacuum distillation system. Soil samples were extracted for approximately 75 minutes and twigs for approximately 55 minutes. The extracted water was then transferred to scintillation vials via pipet and stored at 34°C until analysis.

The hydrogen and oxygen isotope analyses were performed using a Thermo Scientific High Temperature Conversion/Elemental Analyzer (TC/EA) coupled to a

Conflo IV and a Thermo Scientific Delta V Advantage IRMS at the Stable Isotopes for Biosphere Science Laboratory, Texas A&M University. One micro liter (1µl) of sample was injected into TC/EA using a PAL autosampler. The injected sample was converted to H_2 and CO gas by pyrolysis reaction through a glassy carbon tube filled by glassy carbon chips and heated at 1370°C. The H_2 and CO gas were separated by a 2m packed gas chromatograph and were analyzed for the hydrogen and oxygen isotope ratios, respectively, in the Delta V Advantage IRMS. One sample was injected three times. Reported values are an average of these triplicate injections ±0.1‰.

Calibration curves were derived using in-house water standards: SIBS-wA (δ^2H=-390.8 ‰, $\delta^{18}O$=-50.10 ‰) and SIBS-wP (δ^2H=-34.1 ‰, $\delta^{18}O$=-4.60 ‰). Quality control was performed using in-house water standard, SIBS-wU (δ^2H=-120.3 ‰, $\delta^{18}O$=-15.91 ‰). These in-house standards were calibrated using IAEA standards (VSMOW2, SLAP, and GISP) in 2009 and 2014.

f_T Analysis for Sampling Days

To determine how f_T compares between the stable isotope method and the residual of *ET* (ET_{EC} *or* ET_0) and *T,* only data from days when soil and twig samples were collected (to provide real values for the Keeling plots and CGM) were analyzed initially for the growing season (May – October 2019). Four methods were used to calculate f_T: 1) T/ET_{EC}, 2) T/ET_0, 3) δ^2H based stable isotope method, and 4) $\delta^{18}O$ based stable isotope method. This approach was used to provide insight as to how various partitioning methods compare to each other, how δ^2H and $\delta^{18}O$ compare to each other

within the stable isotope method, as well as how the various methods might change over time and with changes in seasonality. Samples were taken for November 2019 to January 2020 as well, however, it was assumed that f_T would be zero during this time due to the trees having entered dormancy and the leaves abscising.

Predictive Model Development

An advantage of this study relative to others like it is the high data resolution and data availability across spatial and temporal scales that are collected by NEON. Due to the high-resolution data that is available throughout the growing season, two models were developed for predicting δ_e and δ_t for all days in the study period based on data from the sampling days. As obtaining soil and twig samples on a daily basis is cumbersome, expensive, and logistically infeasible, this inherently limits the utility of the stable isotope method by limiting the temporal resolution of real values used in the CGM and Keeling plots. However, this barrier may be removed by predicting the isotopic composition of δ_e and δ_t (both δ^2H and $\delta^{18}O$) based on other environmental variables that are easier to measure and do not require on-site presence.

Single and multiple linear regression models were tested using environmental data provided from NEON (air temperature, VPD, soil moisture, precipitation, soil heat flux, net radiation, water vapor concentration, water vapor isotopic composition, wind speed, and relative humidity) to predict the measured isotopic composition of δ_e and δ_t for sampling days during the growing season.

Values from the δ_t predictive models were used directly for δ_T in the isotope method for partitioning ET and values from the δ_e predictive models were used in the

CGM to get δ_E. f_T was then determined every day from May 11th to October 31st for both δ^2H and $\delta^{18}O$.

Results

Environmental Data

The majority of the growing season was characterized by high air temperature (>20°C), stable wind speed, high daytime VPD (>0.3 kPa) and low soil moisture (<0.20 cm^3 cm^{-3}) following storms in May and June (Figure 11). Soil moisture fell consistently between July and September, and this same period experienced the highest daily air temperatures and the least amount of precipitation during the study period. Daytime VPD also reached its maxima in August, indicating peak summer conditions.

However, with the onset of the dormant season at the end of October and beginning of November, air temperature dropped markedly and daily average wind speed showed higher fluctuations without the tree canopy acting as a buffer around the EC tower (Figure 11A). Due to changes with wind speed and air temperature dynamics, daytime VPD also began to drop, relative to growing season conditions (Figure 11B). The beginning of the dormant season was also characterized by a few large rain events that elevated soil moisture levels relative to the summer, and smaller more frequent rain events maintained these higher levels throughout the end of the study.

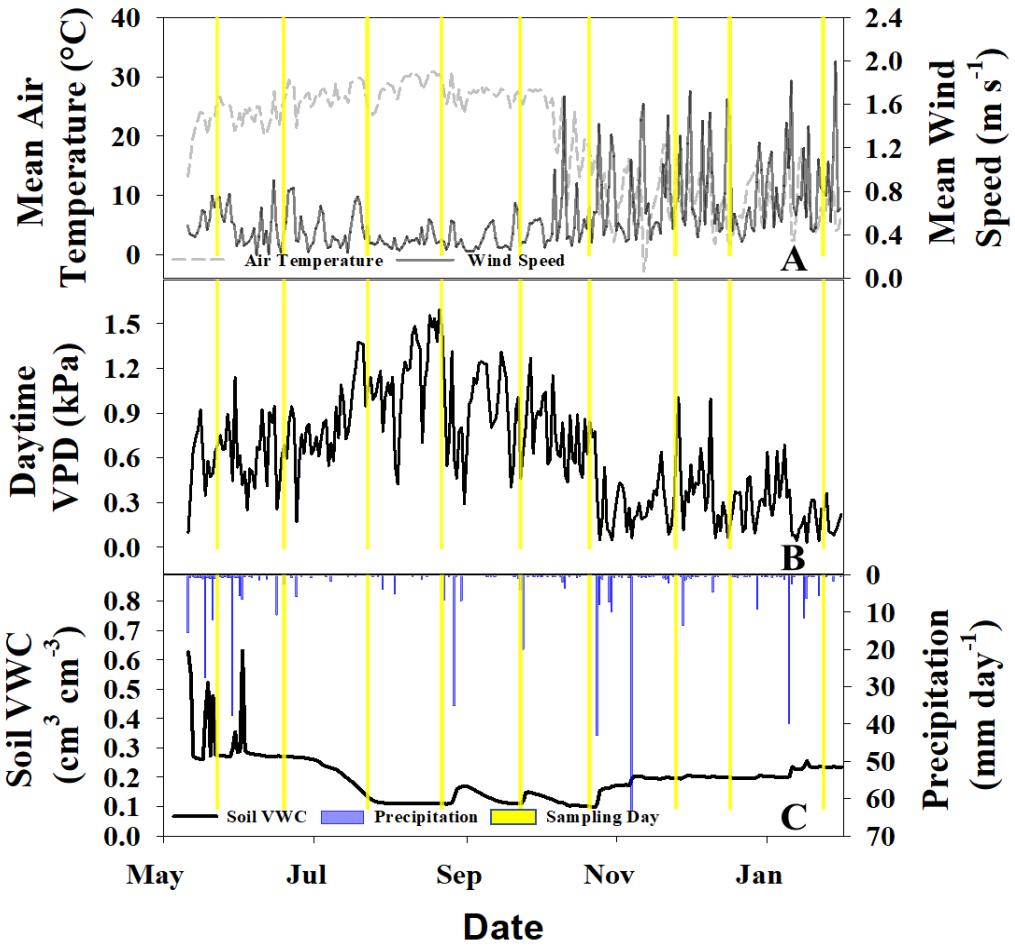

Figure 11. Thirty-minute average air temperature and wind speed recorded from the EC tower during the study period (A), average daytime (6:00-18:00 h) VPD (B), and soil volumetric water content at 0.16-m depth at soil plot 1 (C). Days where there was an isotope sampling event have been highlighted in yellow

Water vapor isotopes also had distinct characteristics during the growing and dormant seasons. While trees were still transpiring, temperatures were still warm, and wind speeds were stable, average water vapor δ^2H and $\delta^{18}O$ was also relatively stable (Figure 12). As trees began to senesce in October and November, resulting in less stomatal conductance, the boundary layer conditions changed and this is reflected in the

higher degree of fluctuations of water vapor isotopes in the dormant season relative to the growing season.

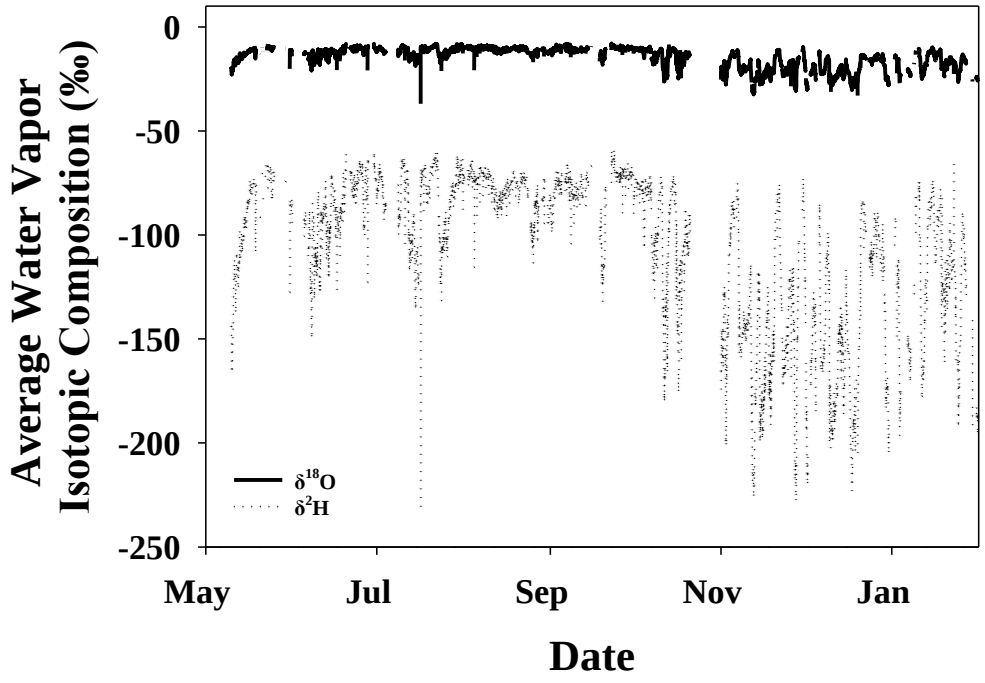

Figure 12. Average isotopic composition of water vapor for the study period. The red line indicates DOY 325 when the trees entered dormancy and leaves abscised.

Water Fluxes

Due to issues with a gas line to the LI-7200 from June to August, actual evapotranspiration (ET_{EC}) was unreliable for the beginning of the study period (Figure 13). However, when the issue was resolved and data was validated, there was moderate agreement for daily evapotranspiration estimated by Penman-Monteith (ET_0) and the eddy covariance method for the remainder of the growing season (2.25±0.89 mm/day and 2.60±0.92 mm day^{-1}, respectively). The eddy covariance method provided sufficient

data 40% of the time from May 11th, 2019 to January 31st, 2020 (107/265 days in the study period) and ET_0 provided sufficient data 88% of the time (233/265 days).

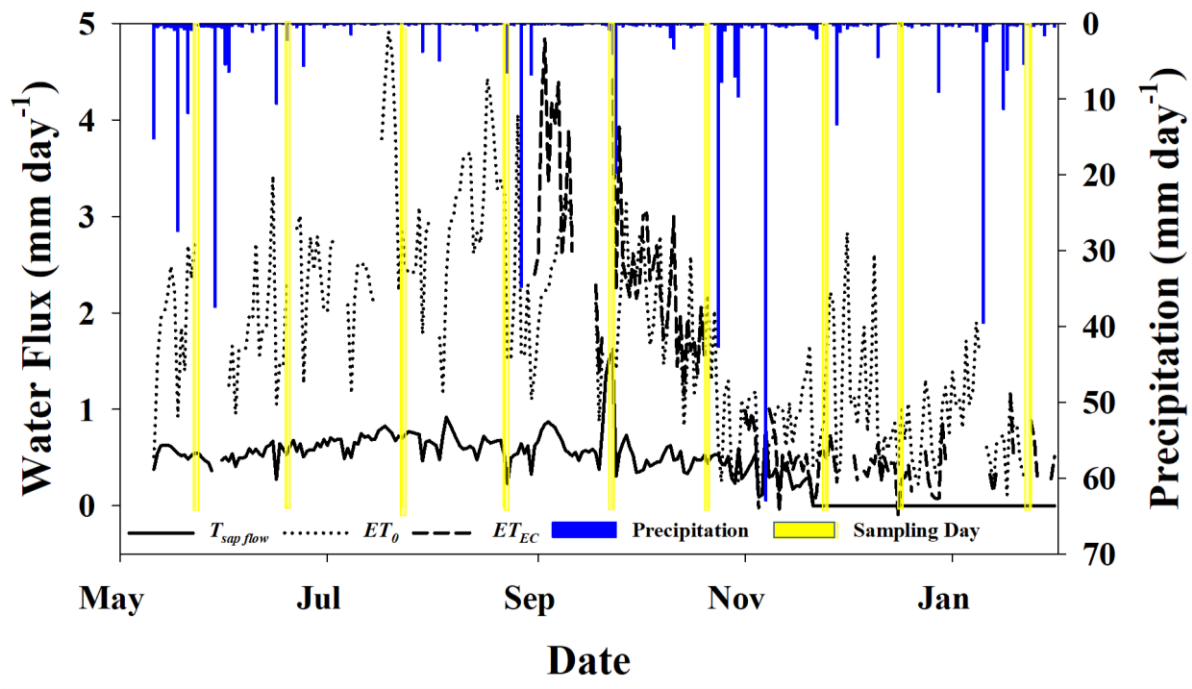

Figure 13. Daily transpiration, reference evapotranspiration, actual evapotranspiration, and precipitation for the study period. Days where there was an isotope sampling event have been highlighted in yellow.

Total precipitation during the measurement period prior to dormancy (May 11th to October 31st) was 315.77 mm, or about 38% of MAP which was 36% below normal for that time of year based on data from the last 50 years (National Weather Service, 2020). Total T, ET_0, and ET_{EC} for this same time period was 102.2 mm (12% of MAP), 391.5 mm (47% of MAP), and 452.4 mm (54% of MAP) respectively. Average transpiration for the growing season was 0.59±0.18 mm day^{-1} and trees were officially deemed dormant on DOY 325 (November 21, 2019) based on sap flow data, just before the November sampling event. Average ET_0 and ET_{EC} for the dormant season

(November-January) was 0.94±0.55 and 0.44±0.28 mm day^{-1}, indicating that ET_0 overestimated total *ET* during this period. This may be due to changes in VPD during this period that bias the Penman-Monteith equation (Figure 11B). All sampling event days had complete water flux data.

Global Meteoric Water Line

To determine if the degree of fractionation between δ^2H and $\delta^{18}O$ should prove feasible for using the stable isotope approach, a global meteoric water line approach (GMWL) was utilized (Figure 14). Atmospheric and precipitation samples fell closely on the line, as was expected. The soil samples fell to the right of the GMWL, indicating preferential evaporation of lighter isotopologues of water and soil enrichment with the heavier isotopologues. These results indicate evaporative fractionation of soil water and an appropriate degree of separation between the signals of twig and soil water isotope ratios, deeming the use of the stable isotope method for partitioning *ET* on sampling days during the growing season feasible.

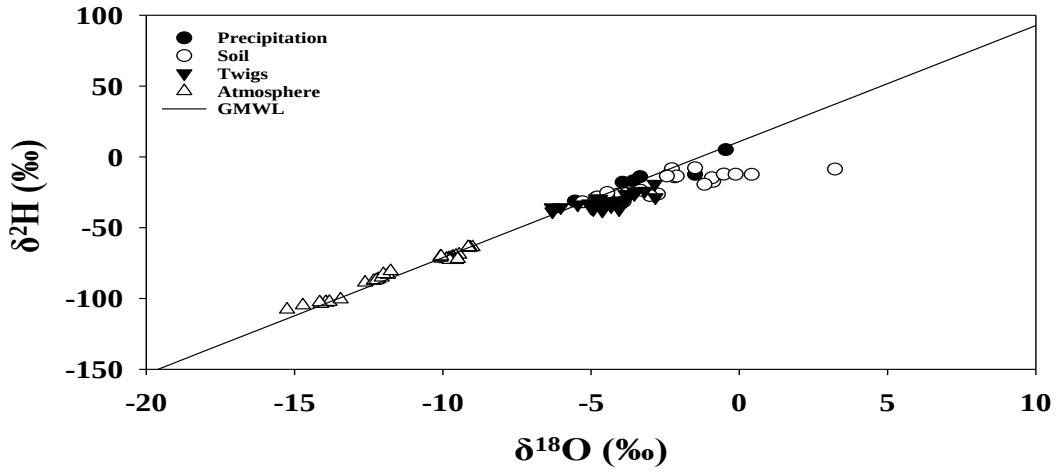

Figure 14. δ^2H versus $\delta^{18}O$ for soil, precipitation, twig, and atmospheric water samples plotted against the GMWL for the growing season.

Keeling Plot

The average of the inverse water concentration between 10:30 - 14:00 h was used against the isotope ratio (both $\delta^{18}O$ and $\delta^{2}H$) during the same time period to construct turbulent mixing relationships, or Keeling plots (Figure 15). All sampling events with the exception of July had significant regression lines and high R^2 values using $\delta^{2}H$ (Table 3). This indicates that the Keeling plot approach is successfully producing a value for δ_{ET} that can be used in Equation 7 for partitioning *ET*. July was also insignificant using $\delta^{18}O$, in addition to the October sampling event. Days when the regression lines were insignificant typically had a change in direction of the slope as well.

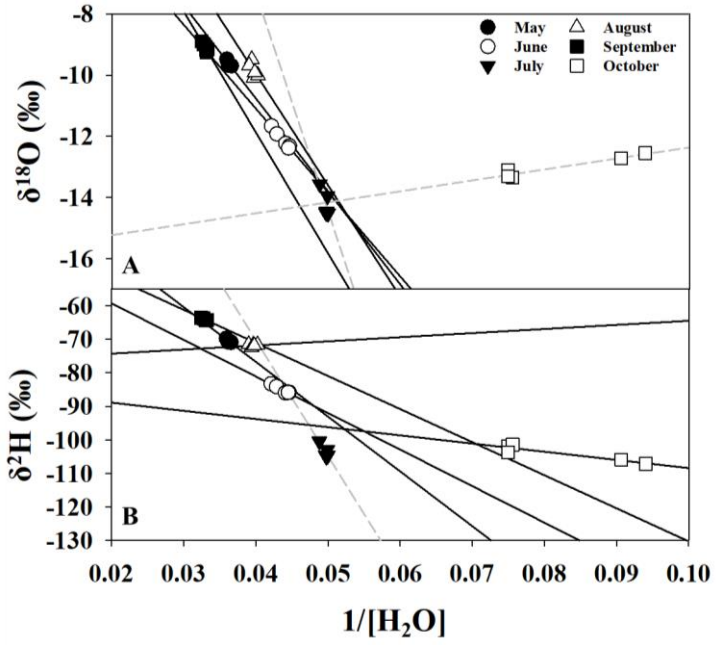

Figure 15. Inverse water vapor concentration plotted against $\delta^{18}O$ (A) and $\delta^{2}H$ (B) for the 6 sampling events during the growing season. Dashed lines represent linear regressions with *P*-values that were non-significant at α=0.05.

Table 3. Descriptive statistics for linear regression (Keeling Plot) analyses for sampling events during the growing season.

		Keeling Plot				
Sampling Day		N	Slope	δ_{ET}	R^2	*P*-Value
5/23/2019	$\delta^{18}O$	21	-236.37	-1.07	0.71	<0.001
	$\delta^{2}H$	21	-1853.90	-3.37	0.77	<0.001
6/19/2019	$\delta^{18}O$	29	-97.11	-7.86	0.61	<0.001
	$\delta^{2}H$	29	-864.74	-47.32	0.86	<0.001
7/23/2019	$\delta^{18}O$	29	109.86	-19.60	0.09	0.11
	$\delta^{2}H$	29	184.18	-112.54	0.02	0.52
8/22/2019	$\delta^{18}O$	29	103.95	-13.95	0.13	0.05
	$\delta^{2}H$	29	-682.05	-44.91	0.57	<0.001
9/23/2019	$\delta^{18}O$	16	-368.38	3.03	0.44	0.005
	$\delta^{2}H$	16	-1084.78	-28.37	0.29	0.03
10/21/2019	$\delta^{18}O$	28	7.11	-13.57	0.03	0.4
	$\delta^{2}H$	28	-331.99	-76.86	0.72	<0.001

f_T

The average f_T calculated from the stable isotope method with data from only sampling days was 0.85±0.27 for $\delta^{18}O$ and 0.7±0.55 for $\delta^{2}H$ (Table 4). On two of the sampling days (May and September) f_T exceeded 100% of total *ET* for both $\delta^{2}H$ and $\delta^{18}O$, indicating that the stable isotope approach may overestimate f_t to some degree. Additionally, the $\delta^{2}H$ July sampling event had a $f_T < 1$, suggesting further issues.

Table 4. Results from *ET* partitioning using the stable isotope approach on sampling days for both $\delta^{2}H$ and $\delta^{18}O$.

	$\delta^{18}O$				$\delta^{2}H$			
Day	δ_{ET}	δ_E	δ_T	f_T	δ_{ET}	δ_E	δ_T	f_T
5/23/2019	-1.07	-43.87	-4.17	1.08	-3.37	-149.94	-28.36	1.21
6/19/2019	-7.86	-43.30	-3.57	0.89	-47.32	-153.45	-24.23	0.82
7/23/2019	-19.60	-30.00	-4.38	0.41	-112.54	-93.24	-32.64	-0.32
8/22/2019	-13.95	-47.00	-4.43	0.78	-44.91	-161.71	-34.59	0.92
9/23/2019	3.03	-48.20	-4.91	1.18	-28.37	-247.21	-32.71	1.02
10/21/2019	-13.57	-40.14	-5.25	0.76	-76.86	-125.57	-37.33	0.55

The average f_T calculated from ET_0 was substantially lower (0.25±0.1) and never went below 0 or above 1 (Figure 16).

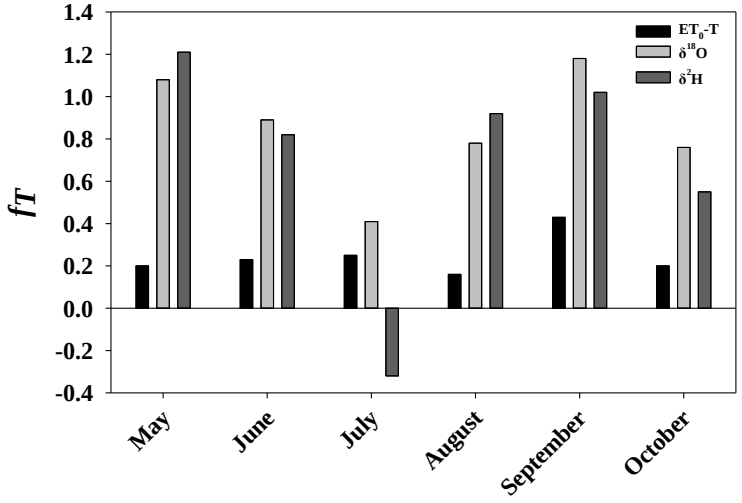

Figure 16. The fractional contribution of transpiration to total evapotranspiration on sampling events during the growing season calculated using the stable isotope method for both δ^2H (dark grey bars) and $\delta^{18}O$ (light grey bars), and using the residual of T/ET_0 from scaled sap flow measurements (black bars).

Values for f_T from T/ET_0 did not compare favorably with f_T from either δ^2H or $\delta^{18}O$ on any sampling day (Figure 16). The f_T of this low-density forest is expected to be around 0.2 - 0.4, which was captured more closely by the traditional method of T/ET_0. On sampling days where Keeling plots were significant, δ^2H and $\delta^{18}O$ performed similarly in magnitude, compared to T/ET_0. The increased data resolution from the CRDS led to a higher utility of both δ^2H and $\delta^{18}O$, indicating that both have the potential to be utilized given a high enough data resolution.

Predictive Model

It was determined that average daytime VPD (between 6:00 - 18:00 h) and average soil moisture at 0.16 m depth were the single best predictors of δ_e and δ_t, respectively (Figure 17). Soil moisture at other depths were tested, however, 0.16 m performed the best and was empirically logical as it is the depth in-between saturated (surface) and unsaturated (0.2 to 0.3-m) sample depths. Raw ‰ values for the individual soil and twig samples from May - January are reported in Appendix B.

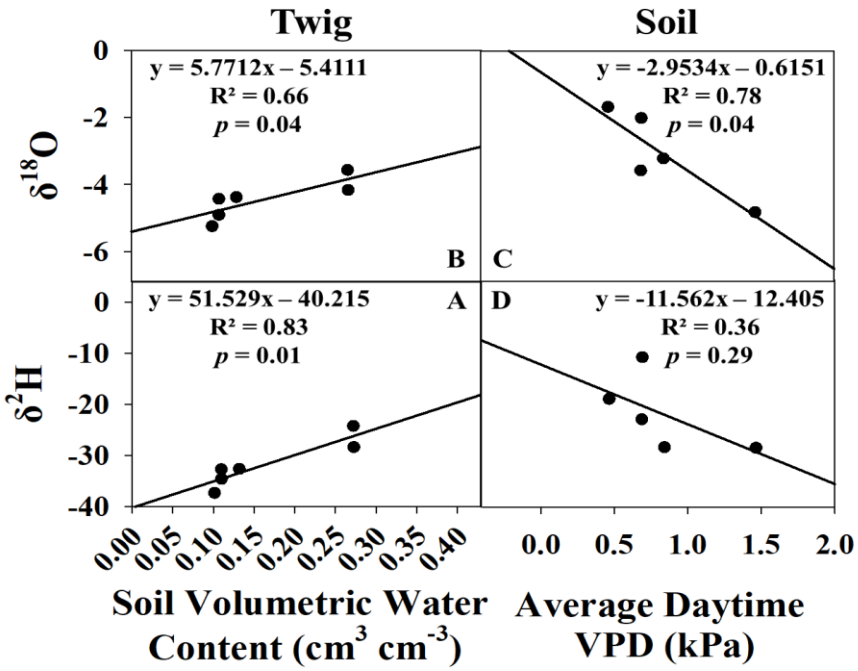

Figure 17. Linear regressions of average soil moisture and twig δ^2H (A), average soil moisture and twig $\delta^{18}O$ (B), average daytime VPD and soil $\delta^{18}O$ (C), and average daytime VPD and soil δ^2H (D) for the growing season only.

Equations from Figure 17 were then used to estimate daily values for soil *E* and vegetation *T* isotopic composition for use in the stable isotope method to partition *ET*.

All models were significant at the 95% confidence level, with the exception of the δ_e δ^2H model. A total of 6 data points were used in the δ_t models, but the July sampling event was excluded from the δ_e models as its Keeling Plot had an insignificant slope (Table 3), and its isotope ratio values were outliers compared to the other 5 months.

Dormant Season Discrepancies

For the dormant season, the same approach was utilized for δ_e and δ_t modeling during the growing season. The additional data from November 2019 - January 2020 was added to the four models and new regressions were conducted. The δ_t models were mostly unaffected and continued to be significant for both δ^2H and $\delta^{18}O$ (Figure 18). However, for the δ_e models the slope of the regression line switched directions, the R^2 values dropped markedly, and the *P*-value for the previously significant $\delta^{18}O$ δ_e model jumped to 0.75.

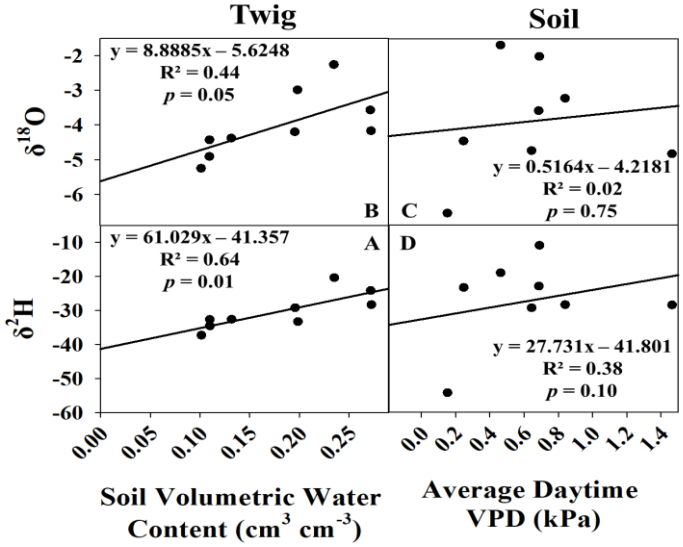

Figure 18. Linear regressions of average soil moisture and twig δ^2H (A), average soil moisture and twig $\delta^{18}O$ (B), average daytime VPD and soil $\delta^{18}O$ (C) and average daytime VPD and soil δ^2H (D) for the growing season data and dormant season data.

Entire Growing Season

Global Meteoric Water Line

When the dormant season data was included with the growing season data on the GMWL, there was still a fair amount of separation between soil and twig isotope ratios, indicating that the stable isotope method for partitioning *ET* should continue to function properly (Figure 19). The precipitation and atmospheric samples were more spread out laterally, but still fell along the line in an appropriate manner.

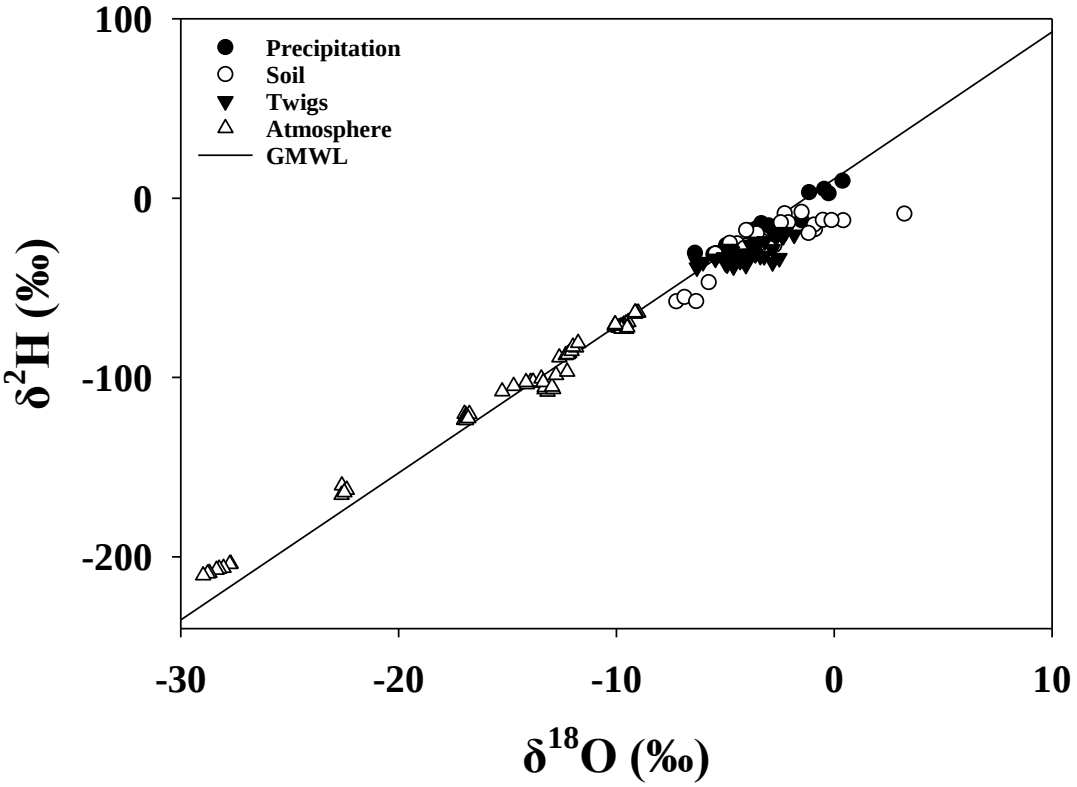

Figure 19. δ^2H versus $\delta^{18}O$ for soil, precipitation, twig, and atmospheric water samples plotted against the GMWL for the growing season and dormant season data.

Keeling Plot

To predict δ_{ET} for the entire growing season, atmospheric isotope data and water vapor concentration data for every day from May 11th 2019 to October 31st 2019 were collected and filtered for data only during 10:30 - 14:00 h for each of the five heights in EC tower. This data was then input into RStudio and underwent linear regression (Keeling plots/turbulent mixing ratios) every day there were sufficient data, for both $\delta^{18}O$ and $\delta^{2}H$. Relevant parameters were extracted for each day, including N, slope, intercept (δ_{ET}), R^2, and a *P*-value which are reported in Appendix C. Of the 164 days in the growing season, there were sufficient EC tower data to construct Keeling plots for 131 days (80%). Of these 131 days with complete data, there were significant slopes for 112 days (86%) using $\delta^{2}H$, and 89 days (68%) using $\delta^{18}O$. Keeling plots were not constructed for the dormant season, due to issues with δ_e modeling and inconsistent atmospheric water vapor concentrations.

Craig-Gordon Model

Of the 164 days in the growing season, the CGM successfully ran for 148 (90%) of days. In this case, $\delta^{18}O$ and $\delta^{2}H$ performed equivalently in terms of producing values for δ_E, and the limiting factor for running the CGM was obtaining complete water vapor isotope data from the EC tower and CRDS. Sixteen days (10%) were missing or had incomplete water vapor isotope data. Relative humidity data were complete for the entire season, as well as soil moisture used to predict δ_e.

f_T

Days with insignificant Keeling plots (P-value > 0.05) were excluded for f_T using the stable isotope method, along with days with f_T < 0 or > 100 for all methods. Day 131 was excluded due to site setup and disturbance. For the first approach (T/ET_{EC}), the average f_T was 0.36 ± 0.31 and there was a total of 70 days (43%) with valid and complete data. For the second approach (T/ET_0), the average f_T was 0.28 ± 0.11 and there was a total of 140 days (86%) with valid and complete data. Both δ^2H and $\delta^{18}O$ had an average f_T of 0.77 ± 0.20, though there were only valid data for 79 and 56 of the 164 days (48% & 34%), respectively. The results from raw calculated f_T are reported in Figure 20.

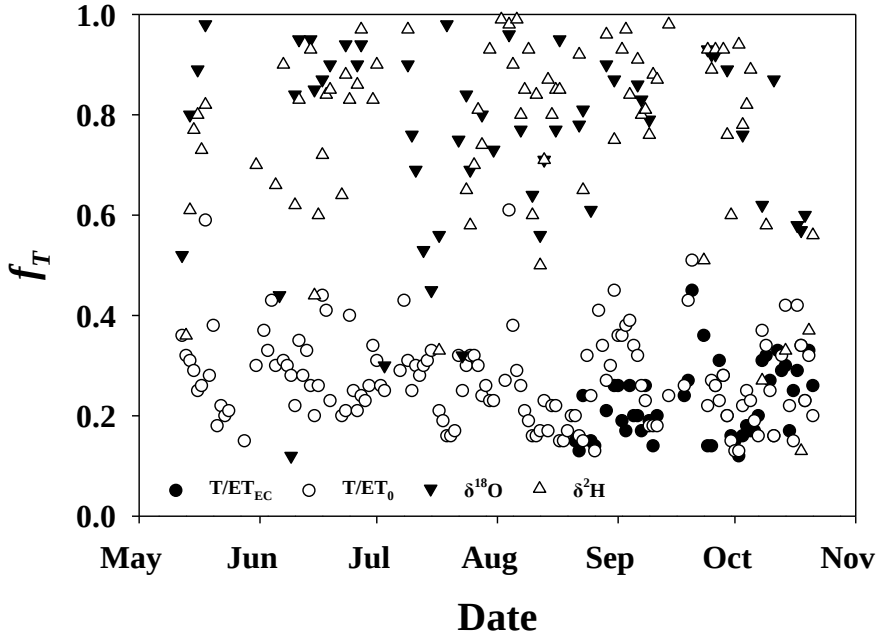

Figure 20. Fractional transpiration computed using T/ET_{EC} (closed circles), T/ET_0 (open circles) δ^2H (open triangles) and $\delta^{18}O$ (closed triangles).

On average, f_T calculated from T/ET_{EC} or T/ET_0 are 41% and 49% lower than those calculated from the stable isotope method. Minimum f_T calculated from the stable isotope method was nearly always greater than maximum value calculated by traditional methods (T/ET_{EC}, T/ET_0). To remove this potential systematic bias from the estimates, f_T from the stable isotope method was normalized to ET_0 (Figure 21A) and ET_{EC} (Figure 21B) to investigate if the trends were similar, despite the absolute magnitude being different. The average ET_0 normalized stable isotope f_T was 0.40 ± 0.15 and the ET_{EC} normalized f_T was 0.32 ± 0.15, which are only 4 - 12% greater than traditional f_T, as opposed to 41-49% before normalization.

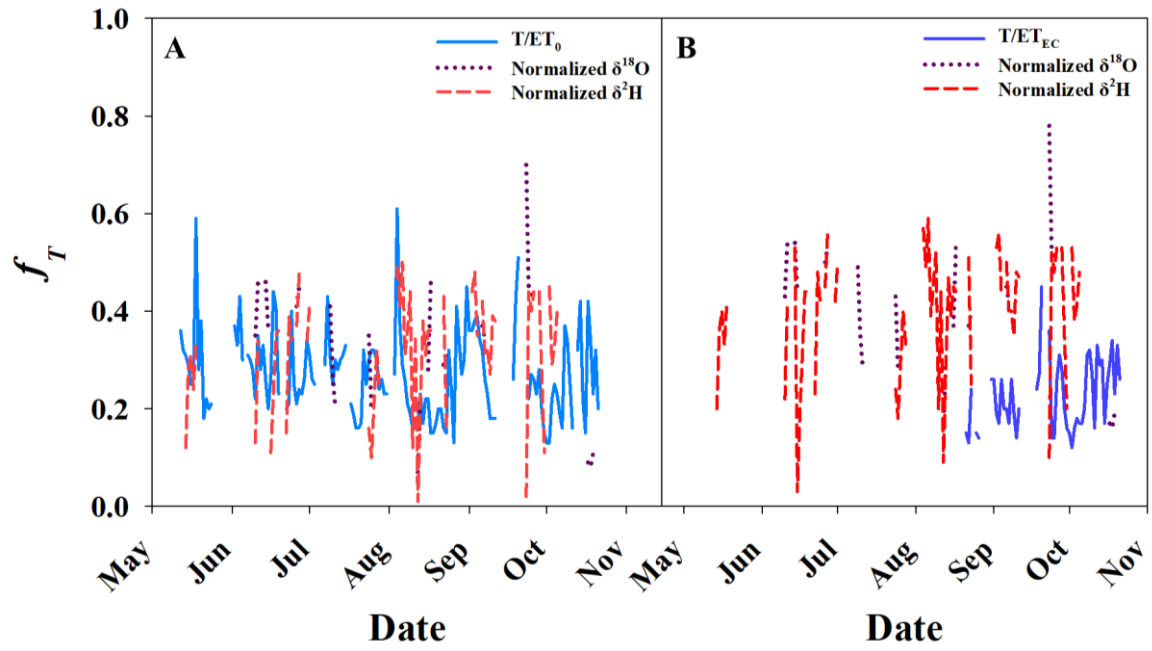

Figure 21. Stable isotope f_T normalized to ET_0 (A) and ET_{EC} (B). Data for ET_{EC} before DOY 241 were invalid and excluded from analysis.

Discussion

This study demonstrated that *ET* can effectively be partitioned using a combination of stable isotopes, sap-flux, and eddy covariance techniques in an oak woodland. The stable isotope technique in particular benefited from improved technological advancements with cavity ringdown spectroscopy and high-temporal resolution vapor collection systems that work in unison with an eddy covariance system. However, the stable isotope method for partitioning *ET* did not compare favorably with more traditional techniques, like using the difference of total *ET* from eddy covariance or ET_0 along with *T* estimated from sap flow measurements. There was a 41 - 49% overestimation of f_T in this system when utilizing the stable isotope technique compared to ET_{EC} or ET_0 relative to sap-flux-based *T*. When using the average difference to normalize f_T for either $\delta^{18}O$ and $\delta^{2}H$ the overestimation was reduced to 4 - 12%, which is within range found from other studies (Williams et al., 2004). This suggests that there may be a systematic bias to the CGM which leads to the overestimation of f_T in natural systems.

When comparing $\delta^{18}O$ and $\delta^{2}H$ within the stable isotope method, there was much agreement between the two, which contrasts with results and conclusions from other studies (Aouade et al. 2016; Williams et al. 2004; Xiao et al. 2018). Typically, $\delta^{2}H$ is utilized over $\delta^{18}O$ due to its higher degree of sensitivity. However, the high temporal-resolution data provided by the CRDS was able to provide the necessary data resolution for $\delta^{18}O$ to perform similarly well. Both $\delta^{18}O$ and $\delta^{2}H$ were able to satisfy requirements for the CGM 90% of the time, and $\delta^{18}O$ only slightly underperformed in the Keeling Plot

approach when compared to δ^2H (68% and 86% of study period). This may be in part to the more sensitive fractionation coefficient for δ^2H relative to $\delta^{18}O$ which increases the potential for significant results, or there may have been evaporation in sample vials during transit from the field to the lab, which can lead to error. However, these results compliment those from the GMWL indicating that stable isotope approach can successfully be utilized within the framework provided in this study. The limiting factors in constructing Keeling plots at the daily scale using the CRDS and the EC tower are having a robust data collection system and a field crew that can maintain and repair the instruments in the case of malfunction or failure. While δ^2H slightly outperformed $\delta^{18}O$, which was expected, $\delta^{18}O$ performed more strongly than previous studies have suggested. This indicates that the high temporal-resolution data collected by the CRDS is truly necessary to make this approach viable at the daily scale for both stable isotopes of water.

A severe limiting factor to the utility of the stable isotope approach for partitioning *ET*, however, is the ability to obtain soil and xylem water samples from the field at fine enough resolutions to examine multi-day or seasonal trends in δ_e and δ_t. For this study, field samples were only feasibly obtained monthly, which limited the data available for partitioning initially to one day per month. However, due to partnership with NEON, a diverse suite of data was available at a much higher resolution and soil and xylem water were successfully modeled using 30-minute vapor pressure deficit and soil moisture data, respectively. This enabled us to partition *ET* from what was initially only 6 sampling events, to 79 and 56 days for δ^2H and $\delta^{18}O$. While this was still only

56% and 48% of all days in the growing season, the stable isotope method was markedly improved by utilizing a combination of modeling and field sampling events. This supports results from Nehemey et al. (2019) who established that tree water status, driven by soil water potential and atmospheric conditions, were the main reasons for source water partitioning and isotopic fractionation during a 7-week lysimeter experiment in Switzerland.

While 0.16-m depth worked best during the growing season for this study, other depths may work better under different precipitation regimes. For instance, if the soil remained constantly saturated during the growing season, then 0.2 to 0.3-m may be more appropriate to model δ_e dynamics. Similarly, under drought conditions it would be more appropriate to model δ_e from soil moisture at the surface. While source water for trees was not independently identified during this study, that may be advantageous in the future to verify the assumption that $\delta_X = \delta_T$. Furthermore, modeled δ_t in this study was based solely off of xylem water from *Quercus spp.* twig samples. However, these values may change if other species in the tower footprint were sampled instead. A more accurate estimation of both *T* and δ_t may be achieved by measuring sap flow in additional species, and sampling those species for xylem water simultaneously.

When dormant season data was added to the δ_e and δ_t models, δ_t remained significant as water inside of the trees were not being utilized during dormancy, however, the δ_e models became unreliable. This suggests that evaporation dynamics during the dormant season are different than during the growing season, and that these dynamics were not successfully captured in the CGM. Furthermore, atmospheric water

vapor isotopes at the onset of and during the dormant season are considerably more variable than during the growing season. This is likely due to the physical barrier that leaves give at the top of the canopy, as well as the regulating properties of active transpiration on the boundary layer micrometeorology, similar to results from Wilson et al. (2000).

It should be noted that forests inherently have more variability and heterogeneity when compared to engineered or agricultural systems like cropland, and this may in part account for variance observed in the boundary layer. However, the combination of insignificant δ_e models and sporadic water vapor concentrations just before and after trees lose their leaves suggest that the Craig-Gordon Model (CGM) cannot be utilized during the dormant season in such systems.

While the application of δ_e and δ_t modeling may be used to interpolate between sampling events during the growing season, the utility of the approach is severely limited during the dormant season due to shifts in boundary layer conditions and evaporation dynamics at the soil surface. Additional experiments with the CGM using high temporal-resolution data collection systems similar to this study are warranted to reconcile discrepancies for CGM performance over changes in season. While in this study the assumption that *T* was negligible during the dormant season may be appropriate, this cannot feasibly be assumed in other ecosystems.

CHAPTER II

CONCLUSIONS

This study has successfully demonstrated that the utility of the stable isotope method for partitioning *ET* in oak woodlands can be markedly improved with integration of high-temporal resolution data collection systems, such as an EC tower coupled with a CRDS, along with field sampling of soil and twigs. The use of both stable isotopes of water is justified when data resolution is high enough, yet the need for normalization to other traditional methods for partitioning *ET* was still necessary. Additional work in natural systems is needed to reconcile this difference in partitioning results, and to test the utility of the proposed δ_e and δ_t models under varying environmental conditions.

REFERENCES

Aouade, G., Ezzahar, J., Amenzou, N., Er-Raki, S., Benkaddour, A., Khabba, S., & Jarlan, L. (2016). Combining stable isotopes, Eddy Covariance system and meteorological measurements for partitioning evapotranspiration, of winter wheat, into soil evaporation and plant transpiration in a semi-arid region. *Agricultural Water Management, 177*, 181-192. doi:https://doi.org/10.1016/j.agwat.2016.07.021

Aparecido, L. M. T., Miller, G. R., Cahill, A. T., & Moore, G. W. (2016). Comparison of tree transpiration under wet and dry canopy conditions in a Costa Rican premontane tropical forest. *30*(26), 5000-5011. doi:doi:10.1002/hyp.10960

Barnes, C. J., & Allison, G. B. (1988). Tracing of water movement in the unsaturated zone using stable isotopes of hydrogen and oxygen. *Journal of Hydrology, 100*(1), 143-176. doi:https://doi.org/10.1016/0022-1694(88)90184-9

Boast, C. W., & Robertson, T. M. (1982). A "Micro-Lysimeter" Method for Determining Evaporation from Bare Soil: Description and Laboratory Evaluation1. *Soil Science Society of America Journal, 46*(4), 689-696. doi:10.2136/sssaj1982.03615995004600040005x

Bowen, I. S. (1926). The Ratio of Heat Losses by Conduction and by Evaporation from any Water Surface. *Physical Review, 27*(6), 779-787. doi:10.1103/PhysRev.27.779

Brunel, J.-P., Walker, G. R., & Kennett-Smith, A. K. (1995). Field validation of isotopic procedures for determining sources of water used by plants in a semi-arid environment. *Journal of Hydrology, 167*(1), 351-368. doi:https://doi.org/10.1016/0022-1694(94)02575-V

Brunel, J. P., Walker, G. R., Dighton, J. C., & Monteny, B. (1997). Use of stable isotopes of water to determine the origin of water used by the vegetation and to partition evapotranspiration. A case study from HAPEX-Sahel. *Journal of Hydrology, 188-189*, 466-481. doi:https://doi.org/10.1016/S0022-1694(96)03188-5

Burba, G. (2013). *Eddy Covariance Method for Scientific, Industrial, Agriculutural, and Regulatory Applications*. Lincoln, Nebraska: LI-COR Biosciences.

Burgess, S. S. O., Adams, M. A., Turner, N. C., Beverly, C. R., Ong, C. K., Khan, A. A. H., & Bleby, T. M. (2001). An improved heat pulse method to measure low and reverse rates of sap flow in woody plants†. *Tree Physiology, 21*(9), 589-598. doi:10.1093/treephys/21.9.589

Cappa, C. D., Hendricks, M. B., DePaolo, D. J., & Cohen, R. C. (2003). Isotopic fractionation of water during evaporation. *Journal of Geophysical Research-Atmospheres, 108*(D16), 10. doi:10.1029/2003jd003597

Čermák, J., Deml, M., & Penka, M. (1973). A new method of sap flow rate determination in trees. *Biologia Plantarum, 15*(3), 171-178. doi:10.1007/bf02922390

Čermák, J., Kučera, J., & Nadezhdina, N. (2004). Sap flow measurements with some thermodynamic methods, flow integration within trees and scaling up from sample trees to entire forest stands. *Trees, 18*(5), 529-546. doi:10.1007/s00468-004-0339-6

Clearwater, M. J., Goldstein, G., Holbrook, N. M., Meinzer, F. C., & Andrade, J. L. (1999). Potential errors in measurement of nonuniform sap flow using heat dissipation probes. *Tree physiology, 19*(10), 681-687.

Cooper, C. E., Morgan, C. L. S., Heilman, J. L., Aparecido, L. M. T., Moore, G. W., & Muir, J. P. (2019). Transpiration in recovering mixed loblolly pine and oak stands following wildfire in the Lost Pines region of Texas. *Ecohydrology, 12*(1). doi:10.1002/eco.2052

Craig, H., & Gordon, L. I. (1965). Δ^2H and oxygen 18 variations in the ocean and the marine atmosphere. In Stable isotopes in oceanographic studies and paleotemperatures. *Δ^2H and Oxygen 18 Variations in the Ocean and the Marine Atmosphere*, 9-130.

Ehleringer, J. R., & Dawson, T. E. (1992). Water uptake by plants: perspectives from stable isotope composition. *Plant, Cell & Environment, 15*(9), 1073-1082. doi:10.1111/j.1365-3040.1992.tb01657.x

Flanagan, L. B., Comstock, J. P., & Ehleringer, J. R. (1991). Comparison of Modeled and Observed Environmental Influences on the Stable Oxygen and Hydrogen Isotope Composition of Leaf Water in Phaseolus vulgaris L. *Plant Physiology, 96*(2), 588. doi:10.1104/pp.96.2.588

Foley, J. A., Costa, M. H., Delire, C., Ramankutty, N., & Snyder, P. (2003). Green surprise? How terrestrial ecosystems could affect earth's climate. *Frontiers in Ecology and the Environment, 1*(1), 38-44. doi:10.1890/1540-9295(2003)001[0038:GSHTEC]2.0.CO;2

Ford, C. R., Hubbard, R. M., Kloeppel, B. D., & Vose, J. M. (2007). A comparison of sap-flux-based evapotranspiration estimates with catchment-scale water balance. *Agricultural and Forest Meteorology, 145*(3), 176-185. doi:https://doi.org/10.1016/j.agrformet.2007.04.010

Gebauer, T., Horna, V., & Leuschner, C. (2008). Variability in radial sap-flux density patterns and sapwood area among seven co-occurring temperate broad-leaved tree species. *Tree Physiology, 28*(12), 1821-1830. doi:10.1093/treephys/28.12.1821

Good, S. P., Moore, G. W., & Miralles, D. G. (2017). A mesic maximum in biological water use demarcates biome sensitivity to aridity shifts. *Nature Ecology & Evolution, 1*(12), 1883-1888. doi:10.1038/s41559-017-0371-8

Granier, A. (1985). Une nouvelle méthode pour la mesure du flux de sève brute dans le tronc des arbres. *Ann. For. Sci., 42*(2), 193-200.

Granier, A. (1987). Evaluation of transpiration in a Douglas-fir stand by means of sap flow measurements. *Tree Physiology, 3*(4), 309-320. doi:10.1093/treephys/3.4.309

He, S., Goodkin, N. F., Jackisch, D., Ong, M. R., & Samanta, D. (2018). Continuous real-time analysis of the isotopic composition of precipitation during tropical rain

events: Insights into tropical convection. *Hydrological Processes, 32*(11), 1531-1545. doi:doi:10.1002/hyp.11520

Helman, D., Lensky, I. M., Osem, Y., Rohatyn, S., Rotenberg, E., & Yakir, D. (2017). A biophysical approach using water deficit factor for daily estimations of evapotranspiration and CO2 uptake in Mediterranean environments. *Biogeosciences, 14*(17), 3909-3926. doi:10.5194/bg-14-3909-2017

Hoff, D. L., Will, R. E., Zou, C. B., & Lillie, N. D. (2018). Encroachment Dynamics of Juniperus virginiana L. and Mesic Hardwood Species into Cross Timbers Forests of North-Central Oklahoma, USA. *Forests (19994907), 9*(2), 75. doi:10.3390/f9020075

Keeling, C. D. (1958). The concentration and isotopic abundances of atmospheric carbon dioxide in rural areas. *Geochimica et Cosmochimica Acta, 13*(4), 322-334. doi:https://doi.org/10.1016/0016-7037(58)90033-4

Keeling, C. D. (1961). The concentration and isotopic abundances of carbon dioxide in rural and marine air. *Geochimica et Cosmochimica Acta, 24*(3), 277-298. doi:https://doi.org/10.1016/0016-7037(61)90023-0

Kljun, N., Calanca, P., Rotach, M. W., & Schmid, H. P. (2015). A simple two-dimensional parameterisation for Flux Footprint Prediction (FFP). *Geosci. Model Dev., 8*(11), 3695-3713. doi:10.5194/gmd-8-3695-2015

Kool, D., Agam, N., Lazarovitch, N., Heitman, J. L., Sauer, T. J., & Ben-Gal, A. (2014). A review of approaches for evapotranspiration partitioning. *Agricultural and*

Forest Meteorology, 184, 56-70. doi:https://doi.org/10.1016/j.agrformet.2013.09.003

Mackay, D. S., Ewers, B. E., Loranty, M. M., & Kruger, E. L. (2010). On the representativeness of plot size and location for scaling transpiration from trees to a stand. *Journal of Geophysical Research-Biogeosciences, 115*, 14. doi:10.1029/2009jg001092

Majoube, M. (1971). Fractionnement en oxygène 18 et en deutérium entre l'eau et sa vapeur. *Journal de Chimie Physique, 68*, 1423-1436. doi: http://dx.doi.org/10.1051/jcp/1971681423

McDowell, N., Barnard, H., Bond, B. J., Hinckley, T., Hubbard, R. M., Ishii, H., . . . Whitehead, D. (2002). The Relationship between Tree Height and Leaf Area: Sapwood Area Ratio. *Oecologia, 132*(1), 12.

Merlivat, L. (1978). Molecular diffusivities of H2 16O, HD16O, and H2 18O in gases. *The Journal of Chemical Physics, 69*(6), 2864-2871. doi:10.1063/1.436884

Moore, G. W., Cleverly, J. R., & Owens, M. K. (2008). Nocturnal transpiration in riparian Tamarix thickets authenticated by sap-flux, eddy covariance and leaf gas exchange measurements. *Tree Physiology, 28*(4), 521-528. doi:10.1093/treephys/28.4.521

Munksgaard, N. C., Wurster, C. M., & Bird, M. I. (2011). Continuous analysis of δ18O and δ2H values of water by diffusion sampling cavity ring-down spectrometry: a novel sampling device for unattended field monitoring of precipitation, ground

and surface waters. *Rapid Communications in Mass Spectrometry, 25*(24), 3706-3712. doi:doi:10.1002/rcm.5282

National Ecological Observatory Network. 2020. Provisional data downloaded from http://data.neonscience.org on 21 Feb 2020. Battelle, Boulder, CO, USA

National Weather Service. 2020. Data accessed on April 21st, 2020. https://www.weather.gov/fwd/dmoprecip

Nehemy, M. F., Benettin, P., Asadollahi, M., Pratt, D., Rinaldo, A., & McDonnell, J. J. (2019). How plant water status drives tree source water partitioning. Hydrol. Earth Syst. Sci. Discuss., 2019, 1-26. doi:10.5194/hess-2019-528

Nier, A. (1991). THE DEVELOPMENT OF A HIGH-RESOLUTION MASS-SPECTROMETER - A REMINISCENCE. *Journal of The American Society for Mass Spectrometry, 2*(6), 447-452.

Perez-Priego, O., El-Madany, T. S., Migliavacca, M., Kowalski, A. S., Jung, M., Carrara, A., . . . Reichstein, M. (2017). Evaluation of eddy covariance latent heat fluxes with independent lysimeter and sapflow estimates in a Mediterranean savannah ecosystem. *Agricultural and Forest Meteorology, 236*, 87-99. doi:https://doi.org/10.1016/j.agrformet.2017.01.009

Pérez-Priego, O., Testi, L., Orgaz, F., & Villalobos, F. J. (2010). A large closed canopy chamber for measuring CO2 and water vapour exchange of whole trees. *Environmental and Experimental Botany, 68*(2), 131-138. doi:https://doi.org/10.1016/j.envexpbot.2009.10.009

Pierchala, A., Rozanski, K., Dulinski, M., Gorczyca, Z., Marzec, M., & Czub, R. (2019). High-precision measurements of δ2H, δ18O and δ17O in water with the aid of cavity ring-down laser spectroscopy. *Isotopes in Environmental and Health Studies, 55*(3), 290-307. doi:10.1080/10256016.2019.1609959

Poyatos, R. C., J; Llorens, P. (2007). Variation in the radial patterns of sap-flux density in pubescent oak (Quercus pubescens) and its implications for tree and stand transpiration measurements. *Tree physiology*(4).

Poyatos, R. L., P.; Gallart, F. (2005). Transpiration of montane Pinus sylvestris L. and Quercus pubescens Willd. forest stands measured with sap flow sensors in NE Spain. *Hydrology and earth system sciences*(5).

R Core Team (2013). R: A language and environment for statistical computing. R Foundation for Statistical Computing, Vienna, Austria. URL http://www.R-project.org/.

Shi, T. T., Guan, D. X., Wu, J. B., Wang, A. Z., Jin, C. J., & Han, S. J. (2008). Comparison of methods for estimating evapotranspiration rate of dry forest canopy: Eddy covariance, Bowen ratio energy balance, and Penman-Monteith equation. *Journal of Geophysical Research-Atmospheres, 113*(D19), 15. doi:10.1029/2008jd010174

Soil Survey Staff, Natural Resources Conservation Service, United States Department of Agriculture. Web Soil Survey. Available online at the following link: https://websoilsurvey.sc.egov.usda.gov/. Accessed January 8, 2019.

Sprenger, M., Leistert, H., Gimbel, K., & Weiler, M. (2016). Illuminating hydrological processes at the soil-vegetation-atmosphere interface with water stable isotopes. *Reviews of Geophysics*, *54*(3), 674-704. doi:10.1002/2015RG000515

Sun, X., Wilcox, B. P., & Zou, C. B. (2019). Evapotranspiration partitioning in dryland ecosystems: A global meta-analysis of in situ studies. *Journal of Hydrology, 576*, 123-136. doi:https://doi.org/10.1016/j.jhydrol.2019.06.022

Tie, Q., Hu, H., Tian, F., & Holbrook, N. M. (2018). Comparing different methods for determining forest evapotranspiration and its components at multiple temporal scales. *Science of The Total Environment, 633*, 12-29. doi:https://doi.org/10.1016/j.scitotenv.2018.03.082

Trenberth Kevin, E., Smith, L., Qian, T., Dai, A., & Fasullo, J. (2007). Estimates of the Global Water Budget and Its Annual Cycle Using Observational and Model Data. *Journal of Hydrometeorology*(4), 758.

Venkatram, A. (1980). Estimating the Monin-Obukhov length in the stable boundary layer for dispersion calculations. *Boundary-Layer Meteorology*, *19*(4), 481-485. doi:10.1007/BF00122347

Vertessy, R. A., Watson, F. G. R., & O′Sullivan, S. K. (2001). Factors determining relations between stand age and catchment water balance in mountain ash forests. *Forest Ecology and Management, 143*(1), 13-26. doi:https://doi.org/10.1016/S0378-1127(00)00501-6

Walker, C. D., & Brunel, J. P. (1990). Examining evapotranspiration in a semi-arid region using stable isotopes of hydrogen and oxygen. *Journal of Hydrology, 118*(1), 55-75. doi:https://doi.org/10.1016/0022-1694(90)90250-2

Wang, L., Caylor, K. K., Villegas, J. C., Barron-Gafford, G. A., Breshears, D. D., & Huxman, T. E. (2010). Partitioning evapotranspiration across gradients of woody plant cover: Assessment of a stable isotope technique. *Geophysical Research Letters, 37*(9). doi:10.1029/2010GL043228

Wilcox, B., Breshears, D., & Seyfried, M. (2003). *Rangelands, Water Balance on*.

Williams, D. G., Cable, W., Hultine, K., Hoedjes, J. C. B., Yepez, E. A., Simonneaux, V., . . . Timouk, F. (2004). Evapotranspiration components determined by stable isotope, sap flow and eddy covariance techniques. *Agricultural and Forest Meteorology, 125*(3), 241-258. doi:https://doi.org/10.1016/j.agrformet.2004.04.008

Wilson, K. B., Hanson, P. J., & Baldocchi, D. D. (2000). Factors controlling evaporation and energy partitioning beneath an oak woodland over an annual cycle. *Agricultural and Forest Meteorology, 102*(2), 83-103. doi:https://doi.org/10.1016/S0168-1923(00)00124-6

Wilson, K. B., Hanson, P. J., Mulholland, P. J., Baldocchi, D. D., & Wullschleger, S. D. (2001). A comparison of methods for determining forest evapotranspiration and its components: sap flow, soil water budget, eddy covariance and catchment water balance. *Agricultural and Forest Meteorology, 106*(2), 153-168. doi:https://doi.org/10.1016/S0168-1923(00)00199-4

Michael, W., & Jan, H. (2013). Biohydrologic effects of eastern redcedar encroachment into grassland, Oklahoma, USA. Biologia, 68(6), 1132-1135. Retrieved from https://www.degruyter.com/view/journals/biolog/68/6/article-p1132.xml. doi:https://doi.org/10.2478/s11756-013-0252-9

Xiao, W., Wei, Z., & Wen, X. (2018). Evapotranspiration partitioning at the ecosystem scale using the stable isotope method—A review. *Agricultural and Forest Meteorology, 263*, 346-361. doi:https://doi.org/10.1016/j.agrformet.2018.09.005

Xiao, X., Horton, R., Sauer, T. J., Heitman, J. L., & Ren, T. (2011). Cumulative Soil Water Evaporation as a Function of Depth and Time. *Vadose Zone Journal, 10*(3), 1016-1022. doi:10.2136/vzj2010.0070

Xu, Z., Yang, H., Liu, F., An, S., Cui, J., Wang, Z., & Liu, S. (2008). Partitioning evapotranspiration flux components in a subalpine shrubland based on stable isotopic measurements. *Botanical Studies, 49*(4), 351-361.

Yakir, D., & Sternberg, L. d. S. L. (2000). The use of stable isotopes to study ecosystem gas exchange. *Oecologia, 123*(3), 297-311. doi:10.1007/s004420051016

Yan, M.-J., Zhang, J.-G., He, Q.-Y., Shi, W.-Y., Otsuki, K., Yamanaka, N., & Du, S. (2016). Sapflow-Based Stand Transpiration in a Semiarid Natural Oak Forest on China's Loess Plateau (Vol. 7).

Yepez, E. A., Williams, D. G., Scott, R. L., & Lin, G. (2003). Partitioning overstory and understory evapotranspiration in a semiarid savanna woodland from the isotopic composition of water vapor. *Agricultural and Forest Meteorology, 119*(1), 53-68. doi:https://doi.org/10.1016/S0168-1923(03)00116-3

Zhang, S., Wen, X., Wang, J., Yu, G., & Sun, X. (2010). The use of stable isotopes to partition evapotranspiration fluxes into evaporation and transpiration. *Acta Ecologica Sinica, 30*(4), 201-209. doi:https://doi.org/10.1016/j.chnaes.2010.06.003

Zimmermann, U., Ehhalt, D., & Muennich, K. O. (1967). *Soil-water movement and evapotranspiration: Changes in the isotopic composition of the water*. International Atomic Energy Agency (IAEA): IAEA.

Zitouna-Chebbi, R., Prévot, L., Chakhar, A., Marniche-Ben Abdallah, M., & Jacob, F. (2018). Observing Actual Evapotranspiration from Flux Tower Eddy Covariance Measurements within a Hilly Watershed: Case Study of the Kamech Site, Cap Bon Peninsula, Tunisia. *Atmosphere, 9*(2), 68.

Zotarelli, L., Dukes, M.D., Romero, C.C., Migliaccio, K.W., Morgan, K.T. (2018). Step by Step Calculation of the Penman-Monteith Evapotranspiration (FAO-56 Method)1. University of Florida IFAS Extension Publication #AE459. Accessed at http://edis.ifas.ufl.edu.

APPENDIX A

INDIVIDUAL VEGETATION PLOT STATISTICS

Plot ID	Type	Stem Count	Sum of Sapwood Area (m^2)	Plot Area (m^2)	Sapwood Area per unit Ground area (m^2 m^{-2})
CLBJ_027	Forest	70	0.764	400	0.00191
CLBJ_028	Forest	51	0.727	400	0.00181
CLBJ_015	Forest	33	0.722	400	0.00180
CLBJ_008	Forest	49	0.594	400	0.00148
CLBJ_029	Forest	20	0.590	400	0.00147
CLBJ_012	Forest	66	0.566	400	0.00141
CLBJ_005	Forest	54	0.506	400	0.00126
CLBJ_014	Forest	77	0.493	400	0.00123
CLBJ_011	Forest	20	0.480	400	0.00120
CLBJ_021	Forest	32	0.469	400	0.00117
CLBJ_002	Forest	74	0.452	400	0.00113
CLBJ_003	Forest	21	0.437	400	0.00109
CLBJ_007	Forest	69	0.435	400	0.00108
CLBJ_026	Forest	43	0.330	400	0.00082
CLBJ_016	Forest	59	0.328	400	0.00082
CLBJ_017	Forest	11	0.306	400	0.00076
CLBJ_009	Forest	31	0.270	400	0.00067
CLBJ_022	Forest	29	0.218	400	0.00054
CLBJ_004	Grass	14	0.101	400	0.00025
CLBJ_010	Grass	6	0.099	400	0.00024
CLBJ_023	Grass	5	0.073	400	0.00018
CLBJ_018	Grass	22	0.065	400	0.00016
CLBJ_006	Grass	21	0.040	400	0.00010
CLBJ_025	Grass	11	0.033	400	8.35078E-05
CLBJ_030	Grass	16	0.021	400	5.36117E-05
CLBJ_019	Grass	5	0.011	400	2.87217E-05
CLBJ_001	Grass	3	0.009	400	2.33471E-05
CLBJ_024	Grass	2	0.001	400	3.55663E-06
CLBJ_020	Grass	1	0.0004	400	1.08381E-06
Averages		31	0.316	400	**0.001208

** Only forest plots were used for averaging.

APPENDIX B

SOIL AND TWIG WATER STABLE ISOTOPE COMPOSITION RESULTS

Sample ID	Material	Average δ^2H (‰)	Average $\delta^{18}O$ (‰)
5/23/2019 LBJ-001	Soil	-14.16 ± 0.35	-2.18 ± 0.33
5/23/2019 LBJ-002	Soil	-8.42 ± 1.45	-2.26 ± 0.38
5/23/2019 LBJ-003	Soil	-7.73 ± 0.85	-1.49 ± 0.41
5/23/2019 LBJ-004	Soil	-13.55 ± 1.5	-2.1 ± 0.34
5/23/2019 LBJ-005	Twig	-26.35 ± 0.86	-3.82 ± 0.34
5/23/2019 LBJ-006	Twig	-31.33 ± 0.69	-4.49 ± 0.37
5/23/2019 LBJ-007	Twig	-29.41 ± 1.84	-4.82 ± 0.46
5/23/2019 LBJ-008	Twig	-26.32 ± 0.91	-3.54 ± 0.41
6/19/2019 LBJ-001	Soil	-23.61 ± 1.75	-3.32 ± 0.34
6/19/2019 LBJ-002	Soil	-26.4 ± 1.77	-4.1 ± 0.52
6/19/2019 LBJ-003	Soil	-13.52 ± 1.5	-2.44 ± 0.33
6/19/2019 LBJ-004	Soil	-28.39 ± 1.62	-4.44 ± 0.52
6/19/2019 LBJ-005	Twig	-29.61 ± 1.4	-4.68 ± 0.39
6/19/2019 LBJ-006	Twig	-23.96 ± 2.9	-3.19 ± 0.1
6/19/2019 LBJ-007	Twig	-24.29 ± 4.87	-3.53 ± 0.54
6/19/2019 LBJ-008	Twig	-19.05 ± 1.83	-2.84 ± 0.44
7/23/2019 LBJ-001	Soil	-12.36 ± 0.56	0.42 ± 0.37
7/23/2019 LBJ-002	Soil	-8.64 ± 3.4	3.22 ± 0.08
7/23/2019 LBJ-003	Soil	-17.31 ± 1.73	-0.88 ± 0.25
7/23/2019 LBJ-004	Soil	-14.79 ± 4.3	-0.92 ± 0.35
7/23/2019 LBJ-005	Twig	-31.83 ± 0.42	-4.08 ± 0.22
7/23/2019 LBJ-006	Twig	-30.87 ± 0.38	-4.02 ± 0.13
7/23/2019 LBJ-007	Twig	-31.75 ± 1.96	-4.42 ± 0.24
7/23/2019 LBJ-008	Twig	-36.11 ± 1.68	-4.99 ± 0.14
8/22/2019 LBJ-001	Soil	-28.58 ± 0.4	-4.8 ± 0.39
8/22/2019 LBJ-002	Soil	-28.34 ± 0.88	-4.78 ± 0.23
8/22/2019 LBJ-003	Soil	-31.86 ± 1.23	-5.27 ± 0.5
8/22/2019 LBJ-004	Soil	-25.22 ± 0.46	-4.45 ± 0.87
8/22/2019 LBJ-005	Twig	-34.89 ± 0.97	-4.31 ± 0.09
8/22/2019 LBJ-006	Twig	-36.96 ± 1.37	-4.91 ± 0.15
8/22/2019 LBJ-007	Twig	-35.48 ± 0.91	-4.64 ± 0.22
8/22/2019 LBJ-008	Twig	-31.02 ± 1.83	-3.83 ± 0.3
9/23/2019 LBJ-001	Soil	-19.39 ± 0.79	-1.16 ± 0.4
9/23/2019 LBJ-002	Soil	-32.46 ± 0.51	-4.89 ± 0.71

9/23/2019 LBJ-003	Soil	-12.15 ± 1	-0.52 ± 0.52
9/23/2019 LBJ-004	Soil	-12.24 ± 0.75	-0.12 ± 0.04
9/23/2019 LBJ-005	Twig	-32.96 ± 0.8	-5.05 ± 0.48
9/23/2019 LBJ-006	Twig	-33.69 ± 2.06	-5.44 ± 0.38
9/23/2019 LBJ-007	Twig	-28.51 ± 0.57	-2.82 ± 0.46
9/23/2019 LBJ-008	Twig	-35.67 ± 0.37	-6.31 ± 0.57
10/21/2019 LBJ-001	Soil	-31.69 ± 1.26	-3.89 ± 0.37
10/21/2019 LBJ-002	Soil	-26.27 ± 0.52	-2.74 ± 0.33
10/21/2019 LBJ-003	Soil	-93.97 ± 1.39	-12.73 ± 0.25
10/21/2019 LBJ-004	Soil	-27.26 ± 1.37	-3 ± 0.11
10/21/2019 LBJ-005	Twig	-35.6 ± 0.76	-6.02 ± 0.2
10/21/2019 LBJ-006	Twig	-38.61 ± 1.06	-6.29 ± 0.49
10/21/2019 LBJ-007	Twig	-37.07 ± 0.29	-4.05 ± 0.29
10/21/2019 LBJ-008	Twig	-38.03 ± 3.21	-4.62 ± 0.23
11/25/2019 LBJ-001	Soil	-27.63 ± 0.64	-4.82 ± 0.1
11/25/2019 LBJ-002	Soil	-30.69 ± 0.42	-5.41 ± 0.47
11/25/2019 LBJ-003	Soil	-31.31 ± 0.69	-4.59 ± 0.34
11/25/2019 LBJ-004	Soil	-27.73 ± 1.23	-4.1 ± 0.27
11/25/2019 LBJ-005	Twig	-28.31 ± 0.52	-4.77 ± 0.19
11/25/2019 LBJ-006	Twig	-26.12 ± 0.14	-3.8 ± 0.05
11/25/2019 LBJ-007	Twig	-31.15 ± 2.37	-3.62 ± 0.46
11/25/2019 LBJ-008	Twig	-31.43 ± 0.47	-4.6 ± 0.2
12/17/2019 LBJ-001	Soil	-57.54 ± 0.15	-7.23 ± 0.36
12/17/2019 LBJ-002	Soil	-55.13 ± 0.42	-6.86 ± 0.4
12/17/2019 LBJ-003	Soil	-57.41 ± 1.58	-6.32 ± 0.29
12/17/2019 LBJ-004	Soil	-46.86 ± 1.62	-5.75 ± 0.21
12/17/2019 LBJ-005	Twig	-35.65 ± 1.16	-2.83 ± 0.35
12/17/2019 LBJ-006	Twig	-33.3 ± 2.39	-2.52 ± 0.64
12/17/2019 LBJ-007	Twig	-32.11 ± 1.26	-3.39 ± 0.28
12/17/2019 LBJ-008	Twig	-32.24 ± 0.67	-3.2 ± 0.46
1-24-2020 LBJ-001	Soil	-30.88 ± 0.75	-5.44 ± 0.1
1-24-2020 LBJ-002	Soil	-25.01 ± 1.25	-4.79 ± 0.54
1-24-2020 LBJ-003	Soil	-19.66 ± 0.93	-3.55 ± 0.41
1-24-2020 LBJ-004	Soil	-17.81 ± 0.51	-4.04 ± 0.37
1-24-2020 LBJ-005	Twig	-21.2 ± 0.81	-2.33 ± 0.41
1-24-2020 LBJ-006	Twig	-20.33 ± 0.22	-1.83 ± 0.47
1-24-2020 LBJ-007	Twig	-21.4 ± 1.87	-2.64 ± 0.48
1-24-2020 LBJ-008	Twig	-18.81 ± 0.49	-2.23 ± 0.52

APPENDIX C

DESCRIPTIVE STATISTICS FOR LINEAR REGRESSION (KEELING PLOT)

ANALYSES FOR EVERY DAY DURING THE GROWING SEASON

		Keeling Plot				
DOY		N	Slope	δ_{ET}	R^2	*P*-Value
131	$\delta^{18}O$	32	-747.52	33.46	0.34	<0.001
	$\delta^{2}H$	32	-7838.76	407.63	0.37	<0.001
132	$\delta^{18}O$	22	-50.06	-13.31	0.52	<0.001
	$\delta^{2}H$	22	-609.83	-78.49	0.66	<0.001
133	$\delta^{18}O$	16	10.49	-14.61	0.10	0.24
	$\delta^{2}H$	16	-552.25	-74.18	0.70	<0.001
134	$\delta^{18}O$	30	-35.49	-10.75	0.21	0.001
	$\delta^{2}H$	30	-615.90	-62.52	0.89	<0.001
135	$\delta^{18}O$	30	-13.70	-11.88	0.04	0.3
	$\delta^{2}H$	30	-776.71	-50.96	0.82	<0.001
136	$\delta^{18}O$	29	-69.80	-8.05	0.61	<0.001
	$\delta^{2}H$	29	-629.38	-50.84	0.59	<0.001
137	$\delta^{18}O$	28	-19.93	-10.25	0.00	0.8
	$\delta^{2}H$	28	-427.45	-62.31	0.27	0.005
138	$\delta^{18}O$	28	-176.00	-3.81	0.29	0.003
	$\delta^{2}H$	28	-792.40	-46.30	0.44	0.001
139	$\delta^{18}O$					
	$\delta^{2}H$					
140	$\delta^{18}O$					
	$\delta^{2}H$					
141	$\delta^{18}O$					
	$\delta^{2}H$					
142	$\delta^{18}O$					
	$\delta^{2}H$					
143	$\delta^{18}O$	21	-236.37	-1.07	0.71	<0.001
	$\delta^{2}H$	21	-1853.90	-3.37	0.77	<0.001
144	$\delta^{18}O$	30	-326.00	0.24	0.20	0.01
	$\delta^{2}H$	30	-2277.56	-1.84	0.19	0.02
145	$\delta^{18}O$	6	-91.11	-6.56	0.08	0.58

	δ^2H	6	785.78	-103.37	0.15	0.46
146	$\delta^{18}O$					
	δ^2H					
147	$\delta^{18}O$					
	δ^2H					
148	$\delta^{18}O$					
	δ^2H					
149	$\delta^{18}O$					
	δ^2H					
150	$\delta^{18}O$					
	δ^2H					
151	$\delta^{18}O$	25	-23.36	-10.21	0.03	0.41
	δ^2H	25	-611.25	-58.20	0.73	<0.001
152	$\delta^{18}O$					
	δ^2H					
153	$\delta^{18}O$					
	δ^2H					
154	$\delta^{18}O$					
	δ^2H					
155	$\delta^{18}O$					
	δ^2H					
156	$\delta^{18}O$	25	62.47	-14.55	0.04	0.32
	δ^2H	25	-907.04	-58.35	0.23	0.01
157	$\delta^{18}O$	22	67.22	-18.39	0.07	0.23
	δ^2H	22	396.78	-125.99	0.03	0.47
158	$\delta^{18}O$	25	-336.03	-2.38	0.20	0.03
	δ^2H	25	-2255.50	-25.01	0.25	0.01
159	$\delta^{18}O$	25	550.91	-36.69	0.62	<0.001
	δ^2H	25	2917.59	-222.64	0.54	<0.001
160	$\delta^{18}O$	21	367.71	-29.36	0.68	<0.001
	δ^2H	21	1396.28	-167.08	0.50	<0.001
161	$\delta^{18}O$	25	-117.65	-9.13	0.38	0.001
	δ^2H	25	-927.70	-57.32	0.40	<0.001
162	$\delta^{18}O$	17	-122.39	-5.69	0.45	0.003
	δ^2H	17	-876.52	-43.51	0.80	<0.001

163	$\delta^{18}O$	9	-403.20	9.02	0.60	0.01
	$\delta^{2}H$	9	-3645.57	98.49	0.60	0.01
164	$\delta^{18}O$	8	-30.42	-9.91	0.05	0.59
	$\delta^{2}H$	8	-305.24	-79.77	0.36	0.12
165	$\delta^{18}O$	21	-105.09	-5.85	0.17	0.06
	$\delta^{2}H$	21	-1077.59	-33.80	0.73	<0.001
166	$\delta^{18}O$	29	-68.88	-9.81	0.18	0.02
	$\delta^{2}H$	29	353.19	-98.74	0.13	0.05
167	$\delta^{18}O$	26	-9.95	-11.60	0.02	0.54
	$\delta^{2}H$	26	-494.01	-65.91	0.72	<0.001
168	$\delta^{18}O$	29	-134.38	-7.20	0.76	<0.001
	$\delta^{2}H$	29	-1052.28	-47.77	0.86	<0.001
169	$\delta^{18}O$	26	9.30	-12.29	0.01	0.68
	$\delta^{2}H$	26	-1100.90	-43.47	0.79	<0.001
170	$\delta^{18}O$	29	-97.11	-7.86	0.61	<0.001
	$\delta^{2}H$	29	-864.74	-47.32	0.86	<0.001
171	$\delta^{18}O$					
	$\delta^{2}H$					
172	$\delta^{18}O$	14	-260.39	-1.77	0.49	0.005
	$\delta^{2}H$	14	-1726.72	-18.29	0.42	0.01
173	$\delta^{18}O$	28	83.43	-12.94	0.03	0.39
	$\delta^{2}H$	28	132.21	-79.87	0.00	0.86
174	$\delta^{18}O$	25	-156.48	-6.49	0.57	<0.001
	$\delta^{2}H$	25	-1261.48	-43.43	0.67	<0.001
175	$\delta^{18}O$	29	-12.93	-9.84	0.05	0.25
	$\delta^{2}H$	29	-287.15	-61.54	0.56	<0.001
176	$\delta^{18}O$	28	-5.95	-9.87	0.00	0.95
	$\delta^{2}H$	28	-254.83	-62.02	0.00	0.75
177	$\delta^{18}O$	19	-138.36	-7.47	0.20	0.05
	$\delta^{2}H$	19	-1290.47	-43.08	0.40	0.003
178	$\delta^{18}O$	26	-123.40	-6.23	0.83	<0.001
	$\delta^{2}H$	26	-1238.07	-31.40	0.90	<0.001
179	$\delta^{18}O$					
	$\delta^{2}H$					
180	$\delta^{18}O$					

	δ^2H					
181	$\delta^{18}O$	28	53.82	-12.60	0.09	0.12
	δ^2H	28	-488.25	-53.63	0.44	<0.001
182	$\delta^{18}O$	29	5.11	-10.78	0.00	0.76
	δ^2H	29	-952.03	-40.64	0.84	<0.001
183	$\delta^{18}O$	28	93.35	-13.59	0.03	0.36
	δ^2H	28	697.32	-95.62	0.02	0.44
184	$\delta^{18}O$	28	448.51	-28.90	0.64	<0.001
	δ^2H	28	1963.94	-161.84	0.54	<0.001
185	$\delta^{18}O$					
	δ^2H					
186	$\delta^{18}O$					
	δ^2H					
187	$\delta^{18}O$					
	δ^2H					
188	$\delta^{18}O$					
	δ^2H					
189	$\delta^{18}O$					
	δ^2H					
190	$\delta^{18}O$	25	-110.15	-7.98	0.73	<0.001
	δ^2H	25	-1486.18	-32.69	0.91	<0.001
191	$\delta^{18}O$	20	180.80	-14.95	0.63	<0.001
	δ^2H	20	188.99	-73.51	0.01	0.64
192	$\delta^{18}O$	26	170.06	-16.84	0.43	<0.001
	δ^2H	26	45.86	-78.27	0.00	0.92
193	$\delta^{18}O$	25	120.23	-19.27	0.05	0.27
	δ^2H	25	377.29	-118.81	0.03	0.44
194	$\delta^{18}O$	25	166.49	-20.58	0.26	0.009
	δ^2H	25	-6.28	-102.01	0.00	0.96
195	$\delta^{18}O$	27	223.42	-22.75	0.02	0.54
	δ^2H	27	1490.86	-161.88	0.02	0.44
196	$\delta^{18}O$	25	173.20	-20.90	0.56	<0.001
	δ^2H	25	129.14	-112.49	0.03	0.39
197	$\delta^{18}O$					
	δ^2H					

198	$\delta^{18}O$	29	392.56	-23.19	0.31	0.002
	$\delta^{2}H$	29	1649.41	-126.19	0.15	0.04
199	$\delta^{18}O$	28	-348.93	2.22	0.74	<0.001
	$\delta^{2}H$	28	-2164.17	3.31	0.77	<0.001
200	$\delta^{18}O$	28	-142.30	-5.27	0.29	0.003
	$\delta^{2}H$	28	-313.93	-64.31	0.05	0.27
201	$\delta^{18}O$	29	-33.64	-8.64	0.02	0.47
	$\delta^{2}H$	29	213.92	-77.79	0.05	0.24
202	$\delta^{18}O$	28	-118.81	-4.32	0.09	0.11
	$\delta^{2}H$	28	-310.36	-53.00	0.11	0.09
203	$\delta^{18}O$	27	167.67	-15.14	0.16	0.04
	$\delta^{2}H$	27	66.77	-69.03	0.00	0.91
204	$\delta^{18}O$	29	137.95	-20.98	0.13	0.05
	$\delta^{2}H$	29	449.88	-125.84	0.09	0.1
205	$\delta^{18}O$	29	-58.30	-10.41	0.04	0.3
	$\delta^{2}H$	29	-756.30	-63.23	0.51	<0.001
206	$\delta^{18}O$	26	76.09	-15.86	0.24	0.01
	$\delta^{2}H$	26	-371.49	-71.02	0.51	<0.001
207	$\delta^{18}O$	29	16.69	-12.80	0.01	0.57
	$\delta^{2}H$	29	-638.76	-61.87	0.72	<0.001
208	$\delta^{18}O$	29	17.79	-11.50	0.02	0.47
	$\delta^{2}H$	29	-527.42	-55.45	0.77	<0.001
209	$\delta^{18}O$	28	67.69	-12.84	0.20	0.02
	$\delta^{2}H$	28	-330.78	-64.86	0.39	<0.001
210	$\delta^{18}O$	26	-335.59	2.62	0.84	<0.001
	$\delta^{2}H$	26	-1179.73	-26.63	0.58	<0.001
211	$\delta^{18}O$	22	-25.78	-8.35	0.03	0.47
	$\delta^{2}H$	22	-793.47	-44.51	0.27	0.01
212	$\delta^{18}O$	9	180.33	-16.00	0.07	0.5
	$\delta^{2}H$	9	-586.41	-50.15	0.03	0.65
213	$\delta^{18}O$					
	$\delta^{2}H$					
214	$\delta^{18}O$	19	21.94	-10.13	0.01	0.73
	$\delta^{2}H$	19	-946.20	-36.42	0.59	<0.001
215	$\delta^{18}O$	24	-932.58	20.06	0.58	<0.001

	δ^2H	24	-3407.79	39.82	0.52	<0.001
216	$\delta^{18}O$	27	-123.32	-6.38	0.16	0.04
	δ^2H	27	-1085.13	-38.14	0.30	0.003
217	$\delta^{18}O$	25	65.14	-12.12	0.05	0.26
	δ^2H	25	-721.36	-48.46	0.42	<0.001
218	$\delta^{18}O$	24	83.10	-11.95	0.11	0.11
	δ^2H	24	-1066.55	-35.26	0.68	<0.001
219	$\delta^{18}O$	27	147.41	-14.41	0.16	0.04
	δ^2H	27	-233.93	-62.42	0.11	0.1
220	$\delta^{18}O$	28	-21.24	-8.64	0.02	0.51
	δ^2H	28	-472.27	-54.14	0.61	<0.001
221	$\delta^{18}O$	25	96.01	-12.43	0.09	0.14
	δ^2H	25	-754.63	-44.07	0.69	<0.001
222	$\delta^{18}O$	26	290.66	-20.15	0.32	0.003
	δ^2H	26	352.81	-85.08	0.15	0.05
223	$\delta^{18}O$	26	149.94	-15.09	0.13	0.08
	δ^2H	26	-545.97	-53.52	0.41	<0.001
224	$\delta^{18}O$	26	339.63	-22.65	0.78	<0.001
	δ^2H	26	399.02	-93.38	0.47	<0.001
225	$\delta^{18}O$	28	160.30	-16.69	0.29	0.003
	δ^2H	28	-428.07	-68.02	0.29	0.003
226	$\delta^{18}O$	22	-92.66	-9.17	0.05	0.3
	δ^2H	22	-1130.41	-49.04	0.27	0.01
227	$\delta^{18}O$	18	61.00	-12.51	0.09	0.23
	δ^2H	18	-546.36	-59.30	0.43	0.003
228	$\delta^{18}O$	28	104.87	-14.04	0.33	0.001
	δ^2H	28	-644.52	-52.87	0.71	<0.001
229	$\delta^{18}O$	19	-112.47	-6.87	0.63	<0.001
	δ^2H	19	-622.51	-53.78	0.77	<0.001
230	$\delta^{18}O$	21	-447.90	5.51	0.31	0.001
	δ^2H	21	-3206.88	39.41	0.40	<0.001
231	$\delta^{18}O$	13	-274.97	-0.84	0.14	0.2
	δ^2H	13	-1837.26	-10.95	0.16	0.18
232	$\delta^{18}O$	11	136.24	-16.37	0.20	0.17
	δ^2H	11	134.67	-84.84	0.01	0.72

233	$\delta^{18}O$	16	76.63	-12.09	0.03	0.52
	$\delta^{2}H$	16	64.43	-74.23	0.00	0.88
234	$\delta^{18}O$	28	100.52	-13.82	0.15	0.04
	$\delta^{2}H$	28	-675.86	-45.09	0.66	<0.001
235	$\delta^{18}O$	27	72.44	-12.77	0.24	0.001
	$\delta^{2}H$	27	334.28	-83.55	0.22	0.01
236	$\delta^{18}O$					
	$\delta^{2}H$					
237	$\delta^{18}O$	27	82.86	-16.82	0.23	0.01
	$\delta^{2}H$	27	29.96	-102.96	0.00	0.88
238	$\delta^{18}O$	28	-316.02	-1.46	0.40	<0.001
	$\delta^{2}H$	28	-2293.86	-10.92	0.44	<0.001
239	$\delta^{18}O$	28	146.58	-18.62	0.06	0.22
	$\delta^{2}H$	28	730.79	-123.11	0.04	0.29
240	$\delta^{18}O$					
	$\delta^{2}H$					
241	$\delta^{18}O$	31	-72.80	-8.27	0.51	<0.001
	$\delta^{2}H$	31	-1320.62	-36.73	0.70	<0.001
242	$\delta^{18}O$					
	$\delta^{2}H$					
243	$\delta^{18}O$	29	-118.52	-8.16	0.71	<0.001
	$\delta^{2}H$	29	-925.22	-56.16	0.27	0.004
244	$\delta^{18}O$	29	27.06	-14.16	0.01	0.59
	$\delta^{2}H$	29	-232.15	-87.63	0.04	0.29
245	$\delta^{18}O$	27	-43.47	-8.73	0.10	0.11
	$\delta^{2}H$	27	-1099.92	-40.36	0.71	<0.001
246	$\delta^{18}O$	28	14.42	-9.79	0.03	0.37
	$\delta^{2}H$	28	-989.84	-35.98	0.81	<0.001
247	$\delta^{18}O$	22	70.97	-12.70	0.09	0.17
	$\delta^{2}H$	22	-636.30	-52.50	0.61	<0.001
248	$\delta^{18}O$					
	$\delta^{2}H$					
249	$\delta^{18}O$	28	36.16	-10.43	0.18	0.02
	$\delta^{2}H$	28	-692.49	-44.28	0.82	<0.001
250	$\delta^{18}O$	23	67.41	-11.73	0.33	0.004

	δ^2H	23	-378.59	-57.25	0.20	0.03
251	$\delta^{18}O$	29	19.90	-11.03	0.01	0.53
	δ^2H	29	-467.24	-55.62	0.46	<0.001
252	$\delta^{18}O$	27	58.38	-12.89	0.21	0.02
	δ^2H	27	-414.68	-61.28	0.66	<0.001
253	$\delta^{18}O$	26	30.99	-11.82	0.04	0.35
	δ^2H	26	-801.58	-47.67	0.55	<0.001
254	$\delta^{18}O$	16	14.35	-11.76	0.00	0.82
	δ^2H	16	-800.81	-49.13	0.30	0.03
255	$\delta^{18}O$	9	7.84	-11.42	0.00	0.94
	δ^2H	9	-874.09	-45.67	0.23	0.19
256	$\delta^{18}O$	6	-318.82	1.68	0.21	0.37
	δ^2H	6	-731.75	-46.83	0.05	0.66
257	$\delta^{18}O$	24	24.43	-11.33	0.06	0.26
	δ^2H	24	-959.28	-36.22	0.83	<0.001
258	$\delta^{18}O$					
	δ^2H					
259	$\delta^{18}O$					
	δ^2H					
260	$\delta^{18}O$					
	δ^2H					
261	$\delta^{18}O$					
	δ^2H					
262	$\delta^{18}O$	27	367.94	-29.64	0.80	<0.001
	δ^2H	27	1713.00	-183.05	0.71	<0.001
263	$\delta^{18}O$	28	-648.44	9.15	0.84	<0.001
	δ^2H	28	-5068.05	75.51	0.84	<0.001
264	$\delta^{18}O$					
	δ^2H					
265	$\delta^{18}O$					
	δ^2H					
266	$\delta^{18}O$	17	-368.38	3.03	0.44	0.005
	δ^2H	17	2256.54	-138.43	0.59	<0.001
267	$\delta^{18}O$	25	-70.53	-7.82	0.25	0.01
	δ^2H	25	-693.16	-48.13	0.31	0.004

268	$\delta^{18}O$	29	-65.49	-8.03	0.40	<0.001
	$\delta^{2}H$	29	-598.62	-50.05	0.77	<0.001
269	$\delta^{18}O$	28	-53.79	-8.00	0.13	0.06
	$\delta^{2}H$	28	-711.34	-41.70	0.66	<0.001
270	$\delta^{18}O$	27	-9.84	-9.97	0.02	0.51
	$\delta^{2}H$	27	-56.08	-65.90	0.02	0.44
271	$\delta^{18}O$	29	-188.51	-3.74	0.37	<0.001
	$\delta^{2}H$	29	-854.94	-41.76	0.28	0.003
272	$\delta^{18}O$	28	-33.19	-8.92	0.14	0.05
	$\delta^{2}H$	28	-136.06	-65.48	0.12	0.08
273	$\delta^{18}O$	25	47.22	-11.75	0.08	0.16
	$\delta^{2}H$	25	441.76	-86.82	0.26	0.009
274	$\delta^{18}O$	22	187.55	-16.76	0.07	0.25
	$\delta^{2}H$	22	44.11	-74.40	0.00	0.97
275	$\delta^{18}O$	28	-175.58	-4.10	0.26	0.006
	$\delta^{2}H$	28	-938.74	-41.19	0.43	<0.001
276	$\delta^{18}O$	28	85.08	-14.03	0.14	0.05
	$\delta^{2}H$	28	-401.61	-59.48	0.23	0.01
277	$\delta^{18}O$	23	-129.06	-8.23	0.16	0.06
	$\delta^{2}H$	23	-1024.87	-52.79	0.21	0.03
278	$\delta^{18}O$	29	-87.82	-7.95	0.07	0.16
	$\delta^{2}H$	29	-867.54	-47.38	0.41	<0.001
279	$\delta^{18}O$	29	141.88	-16.15	0.05	0.26
	$\delta^{2}H$	29	888.00	-113.03	0.06	0.2
280	$\delta^{18}O$	22	31.20	-18.61	0.12	0.12
	$\delta^{2}H$	22	361.58	-140.60	0.39	0.002
281	$\delta^{18}O$	27	42.99	-16.74	0.39	<0.001
	$\delta^{2}H$	27	-172.68	-85.89	0.45	<0.001
282	$\delta^{18}O$	26	-13.44	-12.55	0.02	0.54
	$\delta^{2}H$	26	-424.84	-71.47	0.51	<0.001
283	$\delta^{18}O$	19	759.80	-37.76	0.06	0.33
	$\delta^{2}H$	19	5972.40	-287.30	0.06	0.3
284	$\delta^{18}O$	28	-87.38	-7.99	0.80	<0.001
	$\delta^{2}H$	28	-546.74	-65.51	0.73	<0.001
285	$\delta^{18}O$	18	-9.73	-13.81	0.11	0.18

	δ^2H	18	-160.91	-96.03	0.33	0.01
286	$\delta^{18}O$	14	-49.90	-7.28	0.15	0.17
	δ^2H	14	-231.48	-62.14	0.09	0.29
287	$\delta^{18}O$	12	85.17	-16.67	0.28	0.08
	δ^2H	12	509.24	-113.94	0.32	0.05
288	$\delta^{18}O$	19	2532.48	-101.79	0.45	0.002
	δ^2H	19	17017.94	-689.52	0.44	0.002
289	$\delta^{18}O$	28	-178.15	4.36	0.16	0.04
	δ^2H	28	-602.80	-60.88	0.12	0.08
290	$\delta^{18}O$	29	39.82	-17.30	0.33	0.001
	δ^2H	29	-114.91	-101.67	0.26	0.005
291	$\delta^{18}O$	28	38.02	-17.45	0.24	0.009
	δ^2H	28	-209.97	-85.99	0.45	<0.001
292	$\delta^{18}O$	26	83.44	-18.54	0.23	0.01
	δ^2H	26	409.49	-124.98	0.32	0.002
293	$\delta^{18}O$	28	9.79	-13.79	0.05	0.26
	δ^2H	28	-286.65	-80.68	0.51	<0.001
294	$\delta^{18}O$	27	10.52	-13.87	0.06	0.23
	δ^2H	27	-331.99	-76.86	0.72	<0.001